
Article:
Wang, Wei, Li, Xinrui, Wang, Rui et al. (4 more authors) (2021) Robust 3D-Trajectory and Time Switching Optimization for Dual-UAV-Enabled Secure Communications. IEEE Journal on Selected Areas in Communication. pp. 3334-3347. ISSN: 1558-0008

https://doi.org/10.1109/JSAC.2021.3088628

Robust 3D-Trajectory and Time Switching Optimization for Dual-UAV-Enabled Secure Communications

Wei Wang, *Member, IEEE*, Xinrui Li, Rui Wang, *Senior Member, IEEE*, Kanapathippillai Cumanan, *Senior Member, IEEE*, Wei Feng, *Senior Member, IEEE*, Zhiguo Ding, *Fellow, IEEE*, and Octavia A. Dobre, *Fellow, IEEE*

***Abstract*—This paper investigates a dual-unmanned aerial vehicle (UAV)-enabled secure communication system, in which, a UAV moves around to send confidential messages to a mobile user while another cooperative UAV transmits artificial noise signals to confuse malicious eavesdroppers. Both UAVs have energy constraints and the location information of eavesdroppers is imperfect. We consider a worst-case secrecy rate maximization problem of the mobile user over all time slots. This optimization problem is solved by jointly designing the three-dimensional (3D) trajectory of UAVs and the time allocation (recharging and service or jamming) under practical constraints including maximum UAV speed, UAV collision avoidance, UAV positioning error, and UAV energy harvesting. Specifically, we adopt a more practical UAV-ground channel model with both large-scale and small-scale fading components. Due to the non-convex feasible region constructed by the complicated constraints, directly finding the optimal solution of the original problem is intractable. To address this issue, we decouple the original optimization problem into three subproblems and develop an iterative algorithm to find its suboptimal solution by using the block coordinate descent technique. To solve each subproblem, certain advanced optimization tools, such as integer relaxation, S-procedure, and successive convex approximation techniques, are utilized. Numerical simulation results are provided to corroborate the theoretical derivations and to evaluate the performance of the proposed algorithm. Additionally, the numerical results assist to draw new insights on the 3D UAV trajectory by comparing the performance with conventional two-dimensional (2D) schemes.**

***Index Terms*—Unmanned aerial vehicles (UAV) communications, robust 3D-trajectory design, physical layer security, cooperative jamming, maritime communications.**

W. Wang is with the School of Information Science and Technology, Nantong University, Nantong 226019, China, and with Research Center of Networks and Communications, Peng Cheng Laboratory, Shenzhen 518055, China, and also with the Nantong Research Institute for Advanced Communication Technologies, Nantong 226019, China (e-mail: wwang2011@ntu.edu.cn).

X. Li is with the School of Information Science and Technology, Nantong University, Nantong 226019, China (e-mail:1811310045@yjs.ntu.edu.cn).

R. Wang is with the College of Electronics and Information Engineering, Tongji University, Shanghai 201804, China, and also with the Shanghai Institute of Intelligent Science and Technology, Tongji University, Shanghai 201804, China (e-mail:ruiwang@tongji.edu.cn).

K. Cumanan is with the Department of Electronic Engineering, University of York, York, YO10 5DD, United Kingdom (e-mail:kanapathippillai.cumanan@york.ac.uk).

W. Feng is with the Beijing National Research Center for Information Science and Technology, Department of Electronic Engineering, Tsinghua University, Beijing 100084, China (e-mail:fengwei@tsinghua.edu.cn).

Z. Ding is with the School of Electrical and Electronic Engineering, The University of Manchester, Manchester M13 9PL, United Kingdom (e-mail: zhiguo.ding@manchester.ac.uk).

O. A. Dobre is with the Faculty of Engineering and Applied Science, Memorial University, St. Johns, NL A1B 3X9, Canada (e-mail:odobre@mun.ca)

The work of W. Wang and X. Li were supported in part by the National Natural Science Foundation of China under Grant 61971245, in part by the Six Categories Talent Peak of Jiangsu Province under Grant KTHY-039, in part by the Verification Platform of Multi-tier Coverage Communication Network for oceans under Grant LZC0020, in part by the Science and Technology Program of Nantong under Grant MS22019019, and in part by the Postgraduate Research and Practice Innovation Program of Jiangsu Province under Grant KYCX19-2057. The work of R. Wang was supported in part by the National Natural Science Foundation of China under Grant 61771345 and the project from Shanghai Science and Technology Committee under Grant 19DZ1201102. The work of W. Feng was supported in part by the National Natural Science Foundation of China under Grant 61922049.

I. Introduction

UNMANNED aerial vehicles (UAVs) have attracted significant attention in recent years due to their various potential applications, such as information broadcasting, relaying, and data collection [1]–[4]. This, in contrast to the traditional terrestrial communications, is mainly attributed to the more flexible deployment and agile mobility of UAVs, as well as their line-of-sight (LoS) communication links with the ground terminals at a moderate altitude [5]–[8]. Despite the promising gains and benefits offered by UAVs, the open nature of air-to-ground wireless channels makes the information transfer more vulnerable and a challenging issue [9]. Hence, information security in UAV wireless communications is extremely important and needs to be carefully addressed.

We note that conventional encryption techniques require secret key generations, whose distributions and managements may lead to security vulnerability in wireless systems. On the contrary, physical layer security has recently drawn significant attentions from different wireless communication research communities because of its capability to realize secure transmission by exploiting the inherent randomness and dynamic characteristics of wireless channels [10]–[14]. Recently, different physical layer security techniques have been proposed for providing information security in UAV-assisted communication systems [9], [15]–[17]. Additionally, the fully controllable mobility of UAVs can be exploited to further enhance physical layer security via adjusting its trajectory. This is due to the fact that the UAV can fly close to the legitimate ground node and move away from the eavesdroppers to avoid information interception. Thus, UAV trajectory design has become an important research topic for physical layer security provisioning. For example,

a secrecy rate maximization problem for an UAV-assisted communication system was studied in [18], in which a new trajectory design scheme was proposed by using the mobility of UAV. Physical layer security techniques were extended to both downlink and uplink of an UAV-ground communication system in [19], where the average secrecy rate was maximized by jointly optimizing the trajectory and transmit power of UAV. In [20], a utility optimization problem was considered to maximize the average secrecy rate in UAV-assisted mobile jamming system by jointly designing the UAV's trajectory and jamming power. An average secrecy rate maximization problem for an UAV-enabled secure communication system was studied in [21], where a joint design of UAV trajectory, transmit power levels and power splitting ratios was proposed. Moreover, a UAV-assisted secure system in the presence of multiple eavesdroppers was investigated in [22], where the secrecy rate was maximized by jointly optimizing the trajectory and transmit power of the UAV. However, the authors in [18]–[22] assumed that the locations of eavesdroppers were perfectly known, which is not a realistic assumption, and thus, the results are not applicable to practical scenarios. To deal with this issue, a secure UAV communication system in the presence of multiple eavesdroppers was considered in [23], where a joint robust trajectory design and power control scheme was proposed to maximize the average worst-case secrecy rate.

However, the aforementioned works only considered a single UAV-assisted secure communication system [18]–[23], which may not achieve a high-level security performance. This is because it is generally difficult for an UAV-mounted base station to keep far away from all the eavesdroppers with imperfect knowledge of their locations, when it transmits confidential information to the legitimate receiver. Thus, a cooperative UAV jammer is highly appealing to further improve the quality of secured transmission [24]–[26]. In [24], a dual-UAV enabled secure communication system with multiple eavesdroppers was investigated, where one UAV was assumed to be a mobile base station while the other UAV was considered as a jammer to assist the secure communications of desired users. In [25], the authors considered an UAV-aided secure communication system with a cooperative jamming UAV, where the minimum secrecy rate was maximized by jointly optimizing the trajectory and transmit power of the UAVs as well as the user scheduling. Further, a max-min secrecy rate optimization problem for a dual-UAV enabled secure communication system was studied in [26], in which a joint design of UAV trajectory and transmit power was proposed. However, the authors in [24]–[26] assumed that perfect knowledge of the eavesdroppers' locations is available for trajectory design, which is an impractical assumption. In addition, the aforementioned works, e.g., [18]–[26], assumed that the UAV flies at a fixed altitude and thus only the two-dimensional (2D) UAV trajectory design was considered. In fact, due to fully controllable three-dimensional (3D) mobility, UAVs provide more degrees of freedom to either cruise horizontally or ascend/descend vertically to a desired location, depending on the requirements of communication security. Therefore, designing the 3D trajectory of dual-UAV in the presence of multiple eavesdroppers with imperfect locations is of paramount importance to improve the overall secrecy performance.

Recently, UAV's 3D trajectory design has drawn significant research interests. For instance, in [27], the authors investigated a UAV-enabled wireless sensor network, where the average data collection rate from all sensor nodes was maximized by jointly optimizing the UAV's 3D trajectory and communication scheduling. In [28], a multicarrier solar-powered UAV communication system was considered, where the system sum throughput was maximized by jointly designing the 3D aerial trajectory and the wireless resource allocation over a given time period. A max-min average rate optimization problem for an energy-constrained UAV-assisted downlink cellular network was studied in [29], in which a joint design of resource allocation and 3D trajectory was proposed. In [30], the authors considered a rotary-wing UAV-enabled wireless power transfer system, where the harvested energy at all energy receivers was maximized by jointly optimizing the UAV's 3D trajectory, beam pattern and charging time. Furthermore, in [31], the authors investigated a UAV-assisted cognitive communication network, where the average rate of the secondary receivers was maximized by jointly optimizing the UAV's 3D trajectory and power allocation. Despite the research efforts devoted to the UAV's 3D trajectory design, the existing designs, e.g., [27]–[31], may not be applicable for the use-cases where information security is utmost important in UAV communication systems. It is worth noting that there have been some initial attempts to address the security issues of UAV-assisted communication systems by designing the 3D trajectory. For example, in [32], the authors investigated a secure UAV communication system in the presence of multiple ground nodes and colluding eavesdroppers, where the average secrecy rate was maximized by jointly optimizing the UAV's 3D trajectory and transmit power allocation. However, it was assumed that the locations of eavesdroppers were perfectly known, which is impractical. Furthermore, the works in [27]–[32] only considered the case of a single UAV, which does not provide much degrees of freedom to achieve a better physical layer security performance.

Motivated by the aforementioned aspects, we consider a dual-UAV-assisted secure communication system in this paper, where a UAV base station (UAV-S) intends to send confidential messages to the legitimate mobile user with the help of a cooperative UAV jammer (UAV-J) in the presence of multiple eavesdroppers. In particular, the mobility of both UAVs and user are taken into account. Furthermore, we consider a practical scenario where the eavesdropper's locations are not perfectly known and the onboard energy

TABLE I
LIST OF FUNDAMENTAL VARIABLES.

Symbol	Description
T	Flight period of UAVs
d_t	Length of each time slot
$\alpha[n]$	Time switching (TS) ratio
$\mathbf{q}_a[n]$	Horizontal location of node a
$h_a[n]$	Vertical location of node a
d_{min}	Minimum security distance of UAVs
δ_u	Positioning error at a reference distance
Θ_u	Positioning error threshold of UAVs
$\mathcal{E}_k$	Continuous set of estimation errors
ΔQ_k	Radius of maximum estimation error
$\mathrm{g}_{ab}[n]$	Large-scale channel coefficient between a and b
$\mathrm{h}_{ab}[n]$	Small-scale fading coefficient between a and b
ρ_0	Channel power gain at a reference distance
$d_{ab}[n]$	Distance between a and b
V_a^{max}	Maximum speed of node a
$K[n]$	Rician factor
η	Energy conversion efficiency
ε	Interference cancellation factor
κ	Euler constant
$P_a[n]$	Transmit power of node a
$R_d[n]$	Achievable rate at the mobile user
$R_{e_k}[n]$	Achievable rate at the eavesdroppers
$R_d^{lb}[n]$	Lower bound of $R_d[n]$
$R_{e_k}^{ub}[n]$	Upper bound of $R_{e_k}[n]$
E_u	Minimum EH requirement
Γ_{jd}	Upper bound of small-scale fading between UAV-J and D
Γ_{j^e}	Lower bound of small-scale fading between UAV-J and E_k
$\sigma^2_{\{d,e\}}$	Variance of the additive white Gaussian noise (AWGN)
$\overline{R}_{WCSR}$	Average worst-case secrecy rate

supply of UAVs is limited.[1] Different from most previous works which considered the free space path loss model to simplify the analysis, we adopt a more practical UAV-ground channel model that includes both large-scale and small-scale fading components. Our objective is to maximize the worst-case secrecy rate among all time slots by jointly designing the UAVs 3D trajectory and time switching (TS) (recharging and service or jamming) under the UAV's mobility, anti-collision, positioning and energy harvesting (EH) constraints. To the best of the authors' knowledge, the robust joint design for dual-UAV-assisted secure communications has not been reported in the literature, and our contributions towards the joint design are summarized as follows:

1) We propose a model for a dual-UAV-assisted secure communication system and formulate an optimization problem to maximize the worst-case secrecy rate of the mobile user by taking into account the mobility of both UAVs and mobile user. Additionally, we adopt a more practical UAV-ground channel model with both large-scale and small-scale fading components.

2) Then, we study the joint 3D trajectory and TS design for solving the formulated optimization problem. In order to deal with the non-convexity issue, we decompose the original optimization problem into three subproblems and utilize integer relaxation, S-procedure, and successive convex approximation (SCA) techniques to convert the challenging subproblems into more tractable forms.

3) Next, we develop an iterative optimization algorithm to alternately solve the equivalently converted subproblems by using the block coordinate descent (BCD) method, and then, a suboptimal solution of the original problem is obtained. In each iteration, we derive numerical solutions of the TS ratio, UAV-S and UAV-J trajectories, which provide important insights to incorporate in the efficient system design.

4) Finally, we analyze the convergence and the complexity of the proposed algorithm, and evaluate the system performance through numerical simulations. Furthermore, we show that for the scenario of multiple eavesdroppers and the mobile user, the proposed 3D dual-UAV trajectory can realize a significant secrecy rate gain over the conventional 2D trajectory designs in the literature.

The remainder of the paper is organized as follows. The system model and the problem formulation are presented in Section II, whereas a three-step alternating algorithm is developed in Section III to yield a suboptimal solution for the original optimization problem. Section IV presents simulation results to validate the effectiveness of the proposed design, and finally, Section V concludes the paper.

Notations: Boldface lowercase and uppercase letters denote vectors and matrices, respectively. For a vector $\mathbf{a}$, $\mathbf{a}^\dagger$ and $||\mathbf{a}||$ represents its transpose and Euclidean norm, respectively. $\mathbf{A} \succeq 0$ indicates that $\mathbf{A}$ is a positive semidefinite matrix. $|\cdot|$ and $\mathbb{E}(\cdot)$ denote the absolute value and statistical expectation, respectively. The distribution of a circular symmetric complex Gaussian vector with mean vector $\mathbf{x}$ and covariance matrix $\mathbf{\Sigma}$ is denoted by $\mathcal{CN}(\mathbf{x}, \mathbf{\Sigma})$. The notation $[m]^+$ stands for $\max(0, m)$. A list of variables used in this work is provided in Table I.

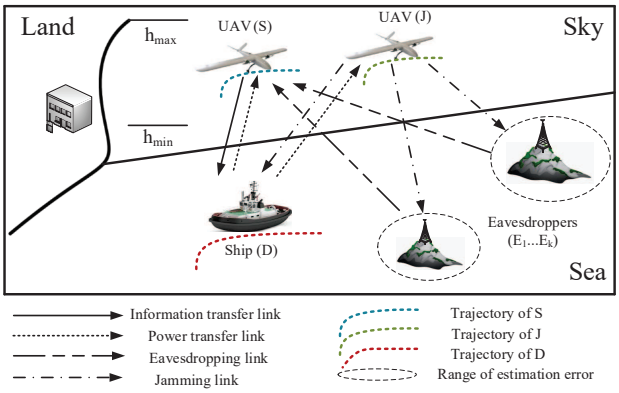

Fig. 1. Illumination of an energy-constrained dual-UAV-assisted secure communication system:a maritime example.

II. SYSTEM MODEL AND PROBLEM FORMULATION

We consider a dual-UAV-assisted secure maritime communication system as shown in Fig. 1, where a UAV-S intends to transmit confidential information to the legitimate mobile user (a ship in the maritime example) D while another UAV-J cooperatively transmits artificial noise (AN) signals to confuse multiple independent eavesdroppers $\{E_1, E_2, \cdots, E_k\}$.

[1]These system settings can occur in emergency communications or ocean scenarios, where the conventional terrestrial base stations are destroyed or do not exist, and then, a mobile aerial base station should be employed to provide the necessary communication infrastructure without the support from a fixed site and power supply.

In practice, the UAVs are connected to shore-based base stations or satellites with wireless backhauls to obtain data and instructions [24]. In this UAV network, it is assumed that UAVs, the mobile user, and all eavesdroppers are equipped with a single antenna [33], [34]. Furthermore, since the UAVs are powered by the energy-limited onboard battery which needs to harvest energy from surrounding environments [28], [35]–[38], we assume that the UAV-S and UAV-J employ the TS protocol to periodically harvest energy from the power-supply D for rendering communication services and cooperative jamming[2]. We consider a particular UAVs flight period with duration T in second (s), which is discretized into N time slots with equal duration $d_t = T/N$, where $\mathcal{N} \triangleq \{1, \cdots, N\}$ denotes the set of slots. Note that the locations of the UAVs can be assumed approximately the same during each time slot when d_t is chosen sufficiently small, as presented in [19], [23], [25], [27]–[29]. Furthermore, let $\alpha[n]$ denote the TS ratio at time slot $n \in \mathcal{N}$, i.e., $\alpha[n] = 0$ and $\alpha[n] = 1$ represents UAVs recharging period and service or jamming period, respectively. Without loss of generality, we consider a 3D cartesian coordinate system, in which the UAVs exploit the fully-controllable mobility to change their 3D locations over time, in order to improve the quality of secrecy communications. The coordinate of the mobile user can be expressed as $(\mathbf{q}_{\mathrm{d}}[n], 0)$, where $\mathbf{q}_{\mathrm{d}}[n] = (x_d[n], y_d[n])$ denotes the horizontal coordinate in time slot n. The coordinates $(\mathbf{q}_{e_k}[n], 0)$, $\mathbf{q}_{e_k}[n] = (x_k[n], y_k[n])$, represent the exact location of the k-th eavesdropper, E_k, $k \in \{1, 2, \cdots, K\}$, which is not available at the legitimate system. However, we assume that the UAVs have the capability to estimate the locations of E_k, i.e., $(x_{e_k}[n], y_{e_k}[n], 0)$ [23], [38]. Furthermore, the time-varying 3D position of dual-UAV can be expressed as $(\mathbf{q}_{\mathrm{u}}[n], h_u[n])$, $u \in \{s, j\}$, where $\mathbf{q}_{\mathrm{u}}[n] = (x_u[n], y_u[n])$ and $h_u[n]$ denote the UAV's horizontal and vertical (or altitude) entries of the 3D coordinate system, respectively. Additionally, suppose that $\mathbf{q}_u[0] = (x_u[0], y_u[0])$ and $\mathbf{q}_u[N] = (x_u[N], y_u[N])$ denote the UAV's pre-determined initial and final horizontal locations, and $h_u[0]$ and $h_u[N]$ denote the corresponding altitudes, respectively. Based on these coordinates, the mobility constraints of the UAVs can be expressed as

$$||\mathbf{q}_{\mathrm{u}}[n] - \mathbf{q}_{\mathrm{u}}[n-1]|| \leq V_{u,h}^{max} d_t, \tag{1a}$$

$$|h_u[n] - h_u[n-1]| \leq V_{u,v}^{max} d_t, \forall n, \tag{1b}$$

where $V_{u,h}^{max}$ and $V_{u,v}^{max}$, $u \in \{s, j\}$, denote the maximum horizontal and vertical speed of UAVs, respectively. Furthermore, to avoid collision between the UAV-S and UAV-J, we impose the following minimum security distance constraint:

$$\sqrt{||\mathbf{q}_{\mathrm{s}}[n] - \mathbf{q}_{\mathrm{j}}[n]||^2 + |h_s[n] - h_j[n]|^2} \geq d_{min}, \forall n \tag{2}$$

where d_{min} is the minimum anti-collision safe distance. Since the UAVs need to correct the positioning error to successfully arrive at the final location in practical scenarios [39], [40], the accumulated errors on the horizontal and vertical directions need to meet the following constraints:

$$\sum_{n=1}^{N} \delta_u ||\mathbf{q}_{\mathrm{u}}[n] - \mathbf{q}_{\mathrm{u}}[n-1]|| \leq \Theta_{u,h}, \tag{3a}$$

$$\sum_{n=1}^{N} \delta_u |h_u[n] - h_u[n-1]| \leq \Theta_{u,v}, \forall n \tag{3b}$$

where δ_u, $u \in \{s, j\}$, denotes the positioning error at a reference distance of 1 m, and $\Theta_{u,h}$ and $\Theta_{u,v}$ represent the horizontal and vertical positioning error thresholds of UAVs, respectively.

As the locations of the eavesdroppers are imperfectly known at the UAVs, the relationships between the actual and the estimated x, y coordinates of E_k can be respectively defined as

$$x_k[n] = x_{e_k}[n] + \Delta x_k[n], \tag{4a}$$

$$y_k[n] = y_{e_k}[n] + \Delta y_k[n], \tag{4b}$$

where $\Delta x_k[n]$ and $\Delta y_k[n]$ denote the estimation errors. These errors are assumed to be bounded within a circle and satisfy the following constraint [23], [38]:

$$\begin{aligned} &(\Delta x_k[n], \Delta y_k[n]) \in \mathcal{E}_k \\ &\triangleq \{(\Delta x_k[n], \Delta y_k[n]) | \Delta x_k^2[n] + \Delta y_k^2[n] \leq \Delta Q_k^2\}, \end{aligned} \tag{5}$$

where $\mathcal{E}_k$ represents a continuous set of possible errors and ΔQ_k^2 denotes the magnitude square of the maximum estimation error. Additionally, it is assumed that the mobile user has a fixed trajectory constraints, which can be defined as[3]

$$x_d[n] = x_d[n-1], y_d[n] = y_d[n-1] + V_d^{max} d_t, \forall n \in \mathcal{N}, \tag{6}$$

where V_d^{max} represents the maximum speed of the mobile user.

In addition to these constraints, different from most previous works which used the free space path loss model to simplify the analysis, a typical UAV-ocean channel model with both large-scale and small-scale fading is employed [33], [34]. Thus, at time slot n, the channel power gains from UAVs to ocean nodes can be defined respectively by

$$\begin{aligned} \mathrm{h}_{ud}[n] &= \mathrm{g}_{ud}[n] \tilde{\mathrm{h}}_{ud}[n] \\ &= (\rho_0 d_{ud}^{-2}[n]) \left(\sqrt{\frac{K[n]}{K[n]+1}} + \sqrt{\frac{1}{K[n]+1}} g_{ud} \right)^2, \end{aligned} \tag{7a}$$

$$\begin{aligned} \mathrm{h}_{ue_k}[n] &= \mathrm{g}_{ue_k}[n] \tilde{\mathrm{h}}_{ue_k}[n] \\ &= (\rho_0 d_{ue_k}^{-2}[n]) \left(\sqrt{\frac{K[n]}{K[n]+1}} + \sqrt{\frac{1}{K[n]+1}} g_{ue_k} \right)^2, \end{aligned} \tag{7b}$$

[2]Since the propulsion energy consumption of the UAV is much larger than that of the wireless transmission in practice, we assume that the onboard battery supplies for the flight control of UAVs while the harvested energy accounts only for its information transmission and cooperative jamming, as commonly adopted in the literature [36]–[38]

[3]This is typical for maritime navigations [33], [34], where all ships have fixed routes to avoid collision. The investigation of multiple mobile users with arbitrary trajectories is an interesting topic for future work.

where $\{\mathrm{g}_{ud}[n], \mathrm{g}_{ue_k}[n]\}$ and $\{\tilde{\mathrm{h}}_{ud}[n], \tilde{\mathrm{h}}_{ue_k}[n]\}$ represent the large-scale and small-scale fading coefficients between UAVs and D as well as E_k, respectively. The symbol ρ_0 denotes the channel power gain at a reference distance of 1 m [18]–[20], [22]–[26], [29], [31], [32], and $d_{ud}[n] = \sqrt{||\mathbf{q}_u[n] - \mathbf{q}_d[n]||^2 + h_u^2[n]}$ and $d_{ue_k}[n] = \sqrt{||\mathbf{q}_u[n] - \mathbf{q}_{e_k}[n]||^2 + h_u^2[n]}$, $u \in \{s, j\}$, represent the distances between UAVs-to-D and UAVs-to-E_k at slot $n \in \mathcal{N}$, respectively. The symbols $\{g_{ud}, g_{ue_k}\} \in \mathcal{CN}(0,1)$ and $K[n]$ defines the Rician factor that corresponds to the ratio between the LoS power and the scattering power[4]. Since the UAVs are powered by an energy-limited onboard battery, it is assumed that the UAVs need to harvest energy for rendering communication services or cooperative jamming. In general, the harvested energy is a nonlinear function with respect to the received radio frequency power [41], [42]. However, there is no generic EH model which can captures all practical scenarios [43]. Therefore, for simplicity, we consider a linear EH model which has been commonly adopted in the literature [22], [28], [29], [38]. Due to $g_{ud} \in \mathcal{CN}(0,1)$, the harvested energy at the UAVs can be expressed as

$$\begin{aligned} E_{EH}^u &= \sum_{n=1}^{N} \mathbb{E}\{(1-\alpha[n])\eta P_d[n]\mathrm{h}_{ud}[n]\} \\ &= \sum_{n=1}^{N} (1-\alpha[n])\eta P_d[n]\mathrm{g}_{ud}[n], \end{aligned} \tag{8}$$

where $P_d[n]$ denotes the transmit power of the mobile user and $\eta \in (0,1]$ represents the energy conversion efficiency. Under the above setting, at time slot $n \in \mathcal{N}$, the signal-to-interference plus-noise ratio (SINR) and the achievable average rate at the mobile user can be defined respectively as

$$\mathrm{SINR}_d[n] = \frac{P_s[n]\mathrm{h}_{sd}[n]}{\sigma_d^2 + \varepsilon P_j[n]\mathrm{h}_{jd}[n]}, \tag{9}$$

and

$$\begin{aligned} R_d[n] &= \mathbb{E}\Big\{\alpha[n]\log_2\Big(1+\mathrm{SINR}_d[n]\Big)\Big\} \\ &\geq \alpha[n]\log_2\Big(1+\frac{e^{-\kappa}P_s[n]\mathrm{g}_{sd}[n]}{\sigma_d^2+\varepsilon P_j[n]\mathrm{g}_{jd}[n]\Gamma_{jd}}\Big) = R_d^{lb}[n], \end{aligned} \tag{10}$$

where $P_s[n]$ and $P_j[n]$ represent the transmit power by the UAV-S and UAV-J, respectively. The symbols ε and κ denote the interference cancellation factor and the Euler constant, respectively. The symbol σ_d^2 represents the variance of the additive white Gaussian noise (AWGN) at the mobile user, and Γ_{jd} denotes the upper bound of small-scale fading between UAV-J and D, and $R_d^{lb}[n]$ represents the lower bound of $R_d[n]$. Similarly, the SINR and the achievable average rate of E_k can be expressed respectively as

$$\mathrm{SINR}_{e_k}[n] = \frac{P_s[n]\mathrm{h}_{se_k}[n]}{\sigma_e^2 + P_j[n]\mathrm{h}_{je_k}[n]}, \tag{11}$$

[4]In general, $K[n]$ is the function of the elevation angle between the UAVs and ground nodes, but it is assumed constant in the current work for tractable analysis, which has been already widely adopted in maritime communication scenarios [33], [34].

and

$$\begin{aligned} R_{e_k}[n] &= \mathbb{E}\Big\{\alpha[n]\log_2\Big(1+\mathrm{SINR}_{e_k}[n]\Big)\Big\} \\ &\leq \alpha[n]\log_2\Big(1+\frac{P_s[n]\mathrm{g}_{se_k}[n]}{\sigma_e^2+P_j[n]\mathrm{g}_{je_k}[n]\Gamma_{je}}\Big) = R_{e_k}^{ub}[n], \end{aligned} \tag{12}$$

where σ_e^2 represents the variance of the AWGN at the k-th eavesdropper, and Γ_{je} denotes the lower bound of small-scale fading between UAV-J and E_k, and $R_{e_k}^{ub}[n]$ represents the upper bound of $R_{e_k}[n]$.

Our objective is to maximize the average worst-case secrecy rate ($\overline{R}_{WCSR}$) among all time slots by jointly designing the dual-UAV 3D trajectory, $\{\mathbf{q}_\mathrm{u}[n], h_u[n]\}$, $u \in \{s, j\}$, and TS ratio $\{\boldsymbol{\alpha}[n]\}$, $\forall n$, subject to the UAV's mobility, anti-collision, positioning and EH constraints. This joint design problem can be formulated as

$$\begin{aligned} \max_{\{\mathbf{q}_\mathrm{u}[n], h_u[n]\}, \boldsymbol{\alpha}[n]} & \frac{1}{N}\sum_{n=1}^{N}\Big[R_d^{lb}[n] \\ & - \max_{k\in\{1,2,\ldots,K\}} \max_{\Delta x_k[n], \Delta y_k[n] \in \mathcal{E}_k} \{R_{e_k}^{ub}[n]\}\Big]^+ \\ \textit{s.t. } & C1: ||\mathbf{q}_\mathrm{u}[n] - \mathbf{q}_\mathrm{u}[n-1]|| \leq V_{u,h}^{max} d_t, u \in \{s,j\}, \forall n, \\ & C2: |h_u[n] - h_u[n-1]| \leq V_{u,v}^{max} d_t, u \in \{s,j\}, \forall n, \\ & C3: \sqrt{||\mathbf{q}_\mathrm{s}[n] - \mathbf{q}_\mathrm{j}[n]||^2 + |h_s[n] - h_j[n]|^2} \geq d_{min}, \forall n, \\ & C4: \sum_{n=1}^{N} \delta_u ||\mathbf{q}_\mathrm{u}[n] - \mathbf{q}_\mathrm{u}[n-1]|| \leq \Theta_{u,h}, u \in \{s,j\}, \forall n, \\ & C5: \sum_{n=1}^{N} \delta_u |h_u[n] - h_u[n-1]| \leq \Theta_{u,v}, u \in \{s,j\}, \forall n, \\ & C6: \sum_{n=1}^{N} (1-\alpha[n])\eta P_d[n]\mathrm{g}_{ud}[n] \geq E_u, u \in \{s,j\}, \forall n, \\ & C7: h_{min} \leq h_u[n] \leq h_{max}, u \in \{s,j\}, \forall n, \\ & C8: \alpha[n] = \{0,1\}, \forall n, \end{aligned} \tag{13}$$

where the constraints C1 and C2 refer to the UAV's mobility constraints and constraint C3 is the security distance constraint between the UAV-S and UAV-J. The constraints C4 and C5 represent the horizontal and vertical positioning error constraint of the UAVs, respectively. E_u in constraint C6 denotes the minimum EH requirement of the UAVs. h_{min} and h_{max} represent the minimum and maximum allowed UAVs flight altitudes, respectively.

Since the problem defined in (13) consists of binary discrete variables ($\boldsymbol{\alpha}[n]$) and highly nonlinear objective function (both numerator and denominator of $R_d^{lb}[n]$ and $R_{e_k}^{ub}[n]$ depend on the optimization variables $\{\mathbf{q}_\mathrm{u}[n], h_u[n]\}$); it is challenging to obtain the global optimal solution. Furthermore, the imperfect locations of the eavesdroppers ($\Delta x_k[n]$, $\Delta y_k[n]$) impose semi-infinite number of constraints, which make the optimization problem mathematically more intractable. In the following section, we propose a computationally efficient iterative al-

gorithm to yield a feasible solution to the problem defined in (13).

III. Proposed Iterative Algorithm

In this section, we resort to the BCD technique through decomposing problem (13) into three subproblems to obtain a suboptimal solution, i.e., alternately optimizing different groups of the TS ratio $\boldsymbol{\alpha}[n]$, UAV-S trajectory $\{\mathbf{q}_\mathrm{s}[n], h_s[n]\}$, and UAV-J trajectory $\{\mathbf{q}_\mathrm{j}[n], h_j[n]\}$ while the rest of the variables are fixed.

A. Optimization of the TS ratio $\boldsymbol{\alpha}[n]$

For given UAV-S and UAV-J 3D trajectories $\{\mathbf{q}_\mathrm{u}[n], h_u[n]\}$, $u \in \{s, j\}$, by relaxing the binary variables in C8 into continuous variables [27], [36], [44], [45], the problem defined in (13) can be equivalently expressed as follows:

$$\max_{\boldsymbol{\alpha}[n]} \ \frac{1}{N}\sum_{n=1}^{N}\alpha[n]M[n] \tag{14a}$$

$$\textit{s.t.} \ \sum_{n=1}^{N}A_1[n]\alpha[n] \le b_1, \tag{14b}$$

$$\sum_{n=1}^{N}A_2[n]\alpha[n] \le b_2, \tag{14c}$$

$$0 \le \alpha[n] \le 1, \forall n, \tag{14d}$$

where

$$M[n] = \log_2\!\left(1+\frac{e^{-\kappa}P_s[n]\mathrm{g}_{sd}[n]}{\sigma_d^2+\varepsilon P_j[n]\mathrm{g}_{jd}[n]\Gamma_{jd}}\right) - \max_{k\in\{1,2,\ldots,K\}}\ \max_{\Delta x_k[n],\Delta y_k[n]\in\mathcal{E}_k}\log_2\!\left(1+\frac{P_s[n]\mathrm{g}_{se_k}[n]}{\sigma_e^2+P_j[n]\mathrm{g}_{je_k}[n]\Gamma_{je}}\right), \tag{15a}$$

$$A_1[n] = \eta P_d[n]\mathrm{g}_{sd}[n], \quad A_2[n] = \eta P_d[n]\mathrm{g}_{jd}[n], \tag{15b}$$

$$b_1 = \sum_{n=1}^{N}\eta P_d[n]\mathrm{g}_{sd}[n] - E_s, b_2 = \sum_{n=1}^{N}\eta P_d[n]\mathrm{g}_{jd}[n] - E_j. \tag{15c}$$

The problem defined in (14) is challenging to be directly solved due to the estimation errors ($\Delta x_k[n]$, $\Delta y_k[n]$) constraints in (15a). Thus, we first define an upper bound for the second term of the right hand side in (15a) as follows:

$$\max_{k\in\{1,2,\ldots,K\}}\ \max_{\Delta x_k[n],\Delta y_k[n]\in\mathcal{E}_k}\log_2\!\left(1+\frac{P_s[n]\mathrm{g}_{se_k}[n]}{\sigma_e^2+P_j[n]\mathrm{g}_{je_k}[n]\Gamma_{je}}\right) \le \log_2\!\left(1+\frac{P_s[n]\mathrm{g}^*_{se}[n]}{\sigma_e^2+P_j[n]\mathrm{g}^*_{je}[n]\Gamma_{je}}\right) \tag{16}$$

where

$$\begin{aligned}\mathrm{g}^*_{se}[n] &= \max_{k\in\{1,2,\ldots,K\}}\ \max_{\Delta x_k[n],\Delta y_k[n]\in\mathcal{E}_k}\ \mathrm{g}_{se_k}[n]\\ &= \max_{k\in\{1,2,\ldots,K\}}\ \mathrm{g}^*_{se_k}[n],\end{aligned} \tag{17a}$$

$$\begin{aligned}\mathrm{g}^*_{je}[n] &= \min_{k\in\{1,2,\ldots,K\}}\ \min_{\Delta x_k[n],\Delta y_k[n]\in\mathcal{E}_k}\ \mathrm{g}_{je_k}[n]\\ &= \min_{k\in\{1,2,\ldots,K\}}\ \mathrm{g}^*_{je_k}[n],\end{aligned} \tag{17b}$$

and then, by substituting (5) and (7) into (17), the closed-form solutions of $\mathrm{g}^*_{se_k}[n]$ and $\mathrm{g}^*_{je_k}[n]$ can be derived as follows:

$$\mathrm{g}^*_{se_k}[n] = \begin{cases}\frac{\rho_0}{h_s^2[n]}, d_{se_k}[n] \le \Delta Q_k,\\ \frac{\rho_0}{(\sqrt{(x_s[n]-x_{e_k}[n])^2+(y_s[n]-y_{e_k}[n])^2}-\Delta Q_k)^2+h_s^2[n]}, d_{se_k}[n] > \Delta Q_k,\end{cases} \tag{18}$$

and

$$\mathrm{g}^*_{je_k}[n] = \frac{\rho_0}{(\sqrt{(x_j[n]-x_{e_k}[n])^2+(y_j[n]-y_{e_k}[n])^2}+\Delta Q_k)^2+h_j^2[n]}. \tag{19}$$

As a result, the lower bound of $M[n]$ in (15a) can be derived and the problem (14) can be reformulated as follows:

$$\begin{aligned} r = \max_{\boldsymbol{\alpha}[n]}\ &\frac{1}{N}\sum_{n=1}^{N}\alpha[n]M^*[n]\\ &\textit{s.t.}\ \text{(14b)} \sim \text{(14d)},\end{aligned} \tag{20}$$

where $M^*[n] = \log_2\!\left(1+\frac{e^{-\kappa}P_s[n]\mathrm{g}_{sd}[n]}{\sigma_d^2+\varepsilon P_j[n]\mathrm{g}_{jd}[n]\Gamma_{jd}}\right) - \log_2\!\left(1+\frac{P_s[n]\mathrm{g}^*_{se}[n]}{\sigma_e^2+P_j[n]\mathrm{g}^*_{je}[n]\Gamma_{je}}\right)$. It is obvious that the reformulated problem in (20) is a standard linear programming problem, which can be efficiently solved by existing standard optimization techniques such as the simplex method [36], [46]. Thus, the optimal solution to the subproblem in (20) can be denoted as

$$\boldsymbol{\alpha}[n] = arg\max_{n}\ r. \tag{21}$$

Remark: Note that the optimal TS ratio $\boldsymbol{\alpha}[n]$ defined in (21) is in general continuous, and can be reconstructed to the binary solution $\{0, 1\}$ using the binarization method in [45] without compromising the optimality of the solution.

B. Optimization of the UAV-S Trajectory $\{\mathbf{q}_\mathrm{s}[n], h_s[n]\}$

With the fixed variables $\boldsymbol{\alpha}[n]$ and $\{\mathbf{q}_\mathrm{j}[n], h_j[n]\}$, the problem defined in (13) can be reformulated as

$$\begin{aligned}\max_{\{\mathbf{q}_\mathrm{s}[n],h_s[n]\}}\ &\frac{1}{N}\sum_{n=1}^{N}\alpha[n]\left[\log_2\!\left(1+\frac{e^{-\kappa}P_s[n]\mathrm{g}_{sd}[n]}{\sigma_d^2+\varepsilon P_j[n]\mathrm{g}_{jd}[n]\Gamma_{jd}}\right)\right.\\ &\left.-\log_2\!\left(1+\frac{P_s[n]\max\limits_{k\in\{1,2,\ldots,K\}}\ \max\limits_{\Delta x_k[n],\Delta y_k[n]\in\mathcal{E}_k}\ \mathrm{g}_{se_k}[n]}{\sigma_e^2+P_j[n]\mathrm{g}_{je}[n]\Gamma_{je}}\right)\right]\\ &\textit{s.t.}\ C1 \sim C7, u = s.\end{aligned} \tag{22}$$

Similar to the previous subproblem in (14), the above problem is also challenging to optimally solve in polynomial time due to its non-convex objective function. To deal with this non-convexity issue, we first introduce a set of slack variables $\mathbf{t}_1 \triangleq [t_1[1], t_1[2], ..., t_1[N]]^\dagger$ and $\mathbf{t}_2 \triangleq [t_2[1], t_2[2], ..., t_2[N]]^\dagger$, and let $g_n = \frac{\rho_0 e^{-\kappa}P_s[n]}{\sigma_d^2+\varepsilon P_j[n]\mathrm{g}_{jd}[n]\Gamma_{jd}}$ and $p_n = \frac{\rho_0 P_s[n]}{\sigma_e^2+P_j[n]\mathrm{g}_{je}[n]\Gamma_{je}}$;

then, the problem defined in (22) reduces to the following problem:

$$\max_{\{x_s[n],y_s[n],h_s[n]\},\mathbf{t}_1,\mathbf{t}_2} \frac{1}{N}\sum_{n=1}^{N}\alpha[n]\Big[\log_2\Big(1+\frac{g_n}{t_1[n]}\Big) - \log_2\Big(1+\frac{p_n}{t_2[n]}\Big)\Big] \tag{23a}$$

$$\text{s.t.} \min_{\Delta x_k[n],\Delta y_k[n]\in\mathcal{E}_k} (x_s[n]-x_k[n])^2+(y_s[n]-y_k[n])^2 +h_s^2[n]\geq t_2[n],\forall n,k, \tag{23b}$$

$$(x_s[n]-x_d[n])^2+(y_s[n]-y_d[n])^2+h_s^2[n]-t_1[n]\leq 0,\forall n, \tag{23c}$$

$$t_2[n]\geq h_{min}^2,\forall n, \tag{23d}$$

$$C1\sim C7, u=s.$$

Note that the problem in (23) is still intractable due to the non-convexity of (23a), (23b) and C6. Therefore, we can leverage the SCA technique to derive its convex approximation [27], as follows. Firstly, by using the first-order Taylor series expansions of $\log_2\Big(1+\frac{g_n}{t_1[n]}\Big)$, we have

$$\log_2\Big(1+\frac{g_n}{t_1[n]}\Big) \geq \log_2\Big(1+\frac{g_n}{t_{1_{fea}}[n]}\Big)-\frac{g_n(t_1[n]-t_{1_{fea}}[n])}{ln2(t_{1_{fea}}^2[n]+g_n t_{1_{fea}}[n])}, \tag{24}$$

where $\mathbf{t}_{1_{fea}}[n]\triangleq[t_{1_{fea}}[1],t_{1_{fea}}[2],...,t_{1_{fea}}[N]]^\dagger$ is the feasible solution obtained at the $(l-1)$th iteration. Then, by introducing a slack variable $\boldsymbol{\xi}_k\triangleq[\xi_k[1],\xi_k[2],...,\xi_k[N]]^\dagger$, based on the proof in Appendix A, (23b) can be equivalently transformed to the following constraints:

$$\widetilde{\boldsymbol{\Phi}}(x_s[n],y_s[n],h_s[n],t_2[n],\xi_k[n])\succeq 0,\forall k,n, \tag{25}$$

where $\widetilde{\boldsymbol{\Phi}}(x_s[n],y_s[n],h_s[n],t_2[n],\xi_k[n]) = \begin{bmatrix} \xi_k[n]+1 & 0 & x_{e_k}[n]-x_s[n] \\ 0 & \xi_k[n]+1 & y_{e_k}[n]-y_s[n] \\ x_{e_k}[n]-x_s[n] & y_{e_k}[n]-y_s[n] & -\Delta Q_k^2\xi_k[n]+\widetilde{c}_k[n]\end{bmatrix}$, and $\widetilde{c}_k[n]=-x_{s_{fea}}^2[n]+2x_{s_{fea}}[n]x_s[n]-2x_{e_k}[n]x_s[n]+x_{e_k}^2[n]-y_{s_{fea}}^2[n]+2y_{s_{fea}}[n]y_s[n]-2y_{e_k}[n]y_s[n]+y_{e_k}[n]^2-h_{s_{fea}}^2[n]+2h_{s_{fea}}[n]h_s[n]-t_2[n]$. Similarly, the constraint C6 in (23) can be equivalently rewritten as follows:

$$\sum_{n=1}^{N}-B_1[n](||(\mathbf{q}_s[n],h_s[n])-(\mathbf{q}_d[n],0)||^2 -||(\mathbf{q}_s[n],h_s[n])^{(l-1)}-(\mathbf{q}_d[n],0)||^2)+B_2[n]\geq E_s. \tag{26}$$

where $B_1[n]=\frac{\eta\rho_0 P_d[n]}{(||(\mathbf{q}_s[n],h_s[n])^{(l-1)}-(\mathbf{q}_d[n],0)||^2)^2}$ and $B_2[n]=\frac{\eta\rho_0 P_d[n]}{||(\mathbf{q}_s[n],h_s[n])^{(l-1)}-(\mathbf{q}_d[n],0)||^2}$.

Based on (24), (25) and (26), the problem defined in (23) can be transformed into an approximated problem in the following form:

$$\max_{\{x_s[n],y_s[n],h_s[n]\},\mathbf{t}_1,\mathbf{t}_2,\boldsymbol{\Xi}} \frac{1}{N}\sum_{n=1}^{N}\alpha[n]\Big[-\frac{g_n(t_1[n]-t_{1_{fea}}[n])}{ln2(t_{1_{fea}}^2[n]+g_n t_{1_{fea}}[n])} -\log_2\Big(1+\frac{p_n}{t_2[n]}\Big)\Big]$$
$$\text{s.t.}\ \ \xi_k[n]\geq 0,\forall k,n,$$
$$C1\sim C5, C7, u=s,$$
$$\text{(23c)},\text{(23d)},(25),(26), \tag{27}$$

where $\boldsymbol{\Xi}\triangleq[\boldsymbol{\xi}_1,\boldsymbol{\xi}_2,...,\boldsymbol{\xi}_K]$. Note that the problem in (27) is a standard semidefinite programming problem, which can be optimally solved by using the interior-point methods [46].

C. Optimization of the UAV-J Trajectory $\{\mathbf{q}_\mathrm{j}[n],h_j[n]\}$

In this subsection, we solve the subproblem for optimizing the 3D trajectory, $\{\mathbf{q}_\mathrm{j}[n],h_j[n]\}$, of UAV-J while the variables $\boldsymbol{\alpha}[n]$ and $\{\mathbf{q}_\mathrm{s}[n],h_s[n]\}$ are fixed. Accordingly, the problem defined in (13) can be equivalently recast as

$$\max_{\{\mathbf{q}_\mathrm{j}[n],h_j[n]\}} \frac{1}{N}\sum_{n=1}^{N}\alpha[n]\Big[\log_2\Big(1+\frac{e^{-\kappa}P_s[n]\mathrm{g}_{sd}[n]}{\sigma_d^2+\varepsilon P_j[n]\mathrm{g}_{jd}[n]\Gamma_{jd}}\Big) -\log_2\Big(1+\frac{P_s[n]\mathrm{g}_{se}[n]}{\sigma_e^2+P_j[n]\Gamma_{je}\min\limits_{k\in\{1,2,...,K\}}\ \min\limits_{\Delta x_k[n],\Delta y_k[n]\in\mathcal{E}_k^\mathrm{g}}\mathrm{g}_{je_k}[n]}\Big)\Big]$$
$$\text{s.t.}\ C1\sim C7, u=j. \tag{28}$$

By introducing new slack variables $\mathbf{m}_1\triangleq[m_1[1],m_1[2],...,m_1[N]]^\dagger$ and $\mathbf{m}_2\triangleq[m_2[1],m_2[2],...,m_2[N]]^\dagger$, and letting $c_n=e^{-\kappa}P_s[n]\mathrm{g}_{sd}[n]$ and $e_n=P_s[n]\mathrm{g}_{se}[n]$, the problem defined in (28) can be equivalently rewritten as

$$\max_{\{x_j[n],y_j[n],h_j[n]\},\mathbf{m}_1,\mathbf{m}_2} \frac{1}{N}\sum_{n=1}^{N}\alpha[n]\Big[\log_2\Big(1+\frac{c_n}{\frac{\rho_0\varepsilon P_j[n]\Gamma_{jd}}{m_1[n]}+\sigma_d^2}\Big) -\log_2\Big(1+\frac{e_n}{\frac{\rho_0 P_j[n]\Gamma_{je}}{m_2[n]}+\sigma_e^2}\Big)\Big] \tag{29a}$$

$$\text{s.t.} \max_{\Delta x_k[n],\Delta y_k[n]\in\mathcal{E}_k} (x_j[n]-x_k[n])^2+(y_j[n]-y_k[n])^2 +h_j^2[n]-m_2[n]\leq 0,\forall k,n, \tag{29b}$$

$$(x_j[n]-x_d[n])^2+(y_j[n]-y_d[n])^2+h_j^2[n]-m_1[n]\geq 0,\forall n, \tag{29c}$$

$$m_1[n]\geq h_{min}^2,\forall n, \tag{29d}$$

$$C1\sim C7, u=j.$$

The reformulated problem in (29) remains still challenging to directly solve due to the non-convexity of (29a), (29b), (29c) and C6. Similar to the previous subproblem, we derive an approximated solution to the problem in (29) by applying the

SCA technique. First, we define an upper bound for the term $\log_2\left(1+\frac{e_n}{\frac{\rho_0 P_j[n]\Gamma_{je}}{m_2[n]}+\sigma_e^2}\right)$ as follows:

$$\log_2\left(1+\frac{e_n}{\frac{\rho_0 P_j[n]\Gamma_{je}}{m_2[n]}+\sigma_e^2}\right)\leq\left(m_2[n]-m_2^{(l-1)}[n]\right)C[n] + \log_2\left(1+\frac{e_n m_2^{(l-1)}[n]}{m_2^{(l-1)}[n]\sigma_e^2+\rho_0 P_j[n]\Gamma_{je}}\right), \tag{30}$$

where $C[n]=\frac{e_n\rho_0 P_j[n]\Gamma_{je}}{ln2(\sigma_e^2 m_2^{(l-1)}[n]+\rho_0 P_j[n]\Gamma_{je})((e_n+\sigma_e^2)m_2^{(l-1)}[n]+\rho_0 P_j[n]\Gamma_{je})}$ and $m_2^{(l-1)}[n]$ is the solution obtained for $m_2[n]$ at the $(l-1)th$ iteration.

Then, the constraint (29b) can be equivalently rewritten based on the geometrical theory as [47]

$$(x_j[n]-x_k^{(l)}[n])^2+(y_j[n]-y_k^{(l)}[n])^2+h_j^2[n]\leq m_2[n],\forall k,n, \tag{31}$$

where $x_k^{(l)}[n]=x_{e_k}[n]-\Delta Q_k\frac{(x_j^{(l-1)}[n]-x_{e_k}[n])}{\sqrt{(x_j^{(l-1)}[n]-x_{e_k}[n])^2+(y_j^{(l-1)}[n]-y_{e_k}[n])^2}}$ and $y_k^{(l)}[n]=y_{e_k}[n]-\Delta Q_k\frac{(y_j^{(l-1)}[n]-y_{e_k}[n])}{\sqrt{(x_j^{(l-1)}[n]-x_{e_k}[n])^2+(y_j^{(l-1)}[n]-y_{e_k}[n])^2}}$.

Finally, similar to (26) and (37), by using the first-order Taylor series expansions of $x_j^2[n]$, $y_j^2[n]$, $h_j^2[n]$ and E_{EH}^j, the constraints (29c) and C6 can be respectively transformed into the following form:

$$\begin{aligned} m_1[n]&+(x_j^{(l-1)}[n])^2+2(x_d[n]-x_j^{(l-1)}[n])x_j[n]-x_d^2[n]\\ &+(y_j^{(l-1)}[n])^2+2(y_d[n]-y_j^{(l-1)}[n])y_j[n]-y_d^2[n]\\ &+(h_j^{(l-1)}[n])^2-2h_j^{(l-1)}[n]h_j[n]\leq 0,\forall n, \end{aligned} \tag{32}$$

and

$$\begin{aligned} \sum_{n=1}^{N}&-B_3[n](||(\mathbf{q}_j[n],h_j[n])-(\mathbf{q}_d[n],0)||^2\\ &-||(\mathbf{q}_j[n],h_j[n])^{(l-1)}-(\mathbf{q}_d[n],0)||^2)+B_4[n]\geq E_j, \end{aligned} \tag{33}$$

where $B_3[n]=\frac{\eta\rho_0 P_d[n]}{(||(\mathbf{q}_j[n],h_j[n])^{(l-1)}-(\mathbf{q}_d[n],0)||^2)^2}$ and $B_4[n]=\frac{\eta\rho_0 P_d[n]}{||(\mathbf{q}_j[n],h_j[n])^{(l-1)}-(\mathbf{q}_d[n],0)||^2}$.

As a result, by substituting (30)−(33) into (29), we rewrite the problem in (29) into an equivalent form as

$$\begin{aligned} \max_{\{x_j[n],y_j[n],h_j[n]\},\mathbf{m}_1,\mathbf{m}_2}\ & \frac{1}{N}\sum_{n=1}^{N}\alpha[n]\left[\log_2\left(1+\frac{c_n}{\frac{\rho_0\varepsilon P_j[n]\Gamma_{jd}}{m_1[n]}+\sigma_d^2}\right)\right.\\ &\left.-(m_2[n]-m_2^{(l-1)}[n])C[n]\right]\\ \text{s.t. }& C1\sim C5, C7, u=j,\\ & (29\text{d}), (31)\sim(33). \end{aligned} \tag{34}$$

It is obvious that the above problem in (34) is a convex optimization problem, which can be efficiently solved by existing standard optimization solvers such as CVX [48].

TABLE II
THE PROPOSED ITERATIVE ALGORITHM.

1: **Set** $l_{max}=100$, $l=0$, $\gamma=10^{-5}$, $R_0^l=0$, and $R_f^l=100$;
2: **Initialize** $\boldsymbol{\alpha}^0$, (x_s^0,y_s^0,h_s^0), and (x_j^0,y_j^0,h_j^0).
3: **While** $R_f^l>\gamma$ and $l<l_{max}$ do;
4: Let $l=l+1$, $x_{sfea}=x_s^{l-1}$, $y_{sfea}=y_s^{l-1}$, and $h_{sfea}=h_s^{l-1}$;
5: Calculate $\boldsymbol{\alpha}^l$ of (20) for given $(x_s^{l-1},y_s^{l-1},h_s^{l-1})$ and $(x_j^{l-1},y_j^{l-1},h_j^{l-1})$;
6: Calculate (x_s^l,y_s^l,h_s^l) of (27) based on $\boldsymbol{\alpha}^l$ and $(x_j^{l-1},y_j^{l-1},h_j^{l-1})$;
7: Calculate (x_j^l,y_j^l,h_j^l) of (34) under given $\boldsymbol{\alpha}^l$ and (x_s^l,y_s^l,h_s^l);
8: Determine $\overline{R}_{WCSR}^l=\frac{1}{N}\sum_{n=1}^{N}(R_d^{lb(l)}[n]-\max_{k\in\{1,2,\ldots,K\}}R_{e_k}^{ub(l)}[n])$ and $R_f^l=|R_0^l-\overline{R}_{WCSR}^l|$;
9: Update $R_o^{l+1}=\overline{R}_{WCSR}^l$;
10: Output $\overline{R}_{WCSR}^*$.

D. Overall Algorithm

In this subsection, based on the results presented in the previous three subsections, we develop an iterative algorithm for problem (13) by applying the BCD method. The proposed algorithm is summarized in Table II and the convergence analysis is given in Appendix B. Furthermore, the overall computational complexity of the proposed algorithm in Table II is as follows. In each iteration of Table II, the problems defined in (20), (27) and (34) in steps 5, 6 and 7 are sequentially optimized using the existing standard convex solvers, and thus their individual complexity can be represented by $\mathcal{O}[N^{3.5}log(1/\varepsilon_0)]$, $\mathcal{O}[(5N+KN)^{3.5}log(1/\varepsilon_0)]$, and $\mathcal{O}[(5N)^{3.5}log(1/\varepsilon_0)]$, respectively. The symbol ε_0 is a given tolerance [14], [27], [49], and K and N denote the numbers of eavesdroppers and time slots, respectively. Thus, the total computation complexity of the proposed algorithm in Table II is $\mathcal{O}[N_{ite}(5N+KN)^{3.5}log(1/\varepsilon_0)]$, where N_{ite} is the number of required iterations, which will be illustrated in the following simulations.

IV. SIMULATION RESULTS

This section provides numerical simulation results to validate the performance of the proposed scheme. The setting of simulation is described in the following. The coordinates of the initial and final locations of the UAVs are set to be $(x_u[0],y_u[0],h_u[0])=(-200,0,100)$ m and $(x_u[N],y_u[N],h_u[N])=(200,0,100)$ m, respectively. The mobile user's (ship) initial horizontal coordinate is $(x_d[n],y_d[n])=(0,200)$ m. It is assumed that there exist two eavesdroppers, whose estimated horizontal coordinates are $(x_{e_1}[n],y_{e_1}[n])=(-100,-200)$ m and $(x_{e_2}[n],y_{e_2}[n])=(100,-250)$ m, respectively. Furthermore, the channel power gain ρ_0 is 40 dBm [23], the Rician factor $K[n]$ is 31.3, and the upper and lower bounds of small-scale fading are assumed to be $\Gamma_{jd}=1.35$ and $\Gamma_{je}=0.65$, respectively [33]. Moreover, unless otherwise specified, $\eta=0.8$ is the energy conversion efficiency, $\sigma_d^2=\sigma_e^2=-30$ dBm are the noise variances, $\Delta Q_1=\Delta Q_2=20$ m are the estimation errors radii, $P_d[n]=25$ dBm is the transmit power at the mobile user, $P_s[n]=P_j[n]=20$ dBm are the transmit

power at the UAV-S and UAV-J, respectively [24], [25]. Additionally, $\delta_s = \delta_j = 0.01$ are the positioning errors and $\Theta_{u,h} = \Theta_{u,v} = 20$ are the horizontal and vertical positioning error thresholds of UAVs. In addition, $V_d^{max} = 15$ m/s is the maximum speed of the mobile user, $V_{u,h}^{max} = 20$ m/s and $V_{u,v}^{max} = 20/\sqrt{2}$ m/s, $u \in \{s, j\}$, are the maximum horizontal and vertical speed of the UAV-S and UAV-J, $h_{min} = 20$ m and $h_{max} = 120$ m are the minimum and maximum UAVs flight altitudes, respectively [27], [29], [32].

Fig. 2(a) and Fig. 2(b) depict the projections of the trajectories of the UAVs onto the horizontal plane and the 3D plane during different time durations T, respectively. The initial location of the mobile user D is marked by $*$ and the exact locations of the eavesdroppers E_n are marked by $\times$. $\triangle$ and $\bigtriangledown$ denote the initial and final positions of the UAV-S and UAV-J, respectively. As can be seen in Fig. 2(a), when T is small (e.g., $T = 21$ s), both UAV-S (solid curves) and UAV-J (dashed curves) almost directly fly to the final location, since the minimum flight time T is required to fly from the initial location to the final location. As T increases, the UAV-S first flies in an arc path to keep away from the eavesdropper E_1, then it follows the mobile user as long as possible, and finally flies to the final location along an arc path bypassing the eavesdropper E_2. Meanwhile, the UAV-J first exploits its mobility to move closer to the eavesdroppers, then it hovers over the center of the estimated locations of the eavesdroppers as long as possible, and finally flies quickly to the final location. The reason behind this behavior is that UAV-S needs to follow the mobile user to harvest sufficient energy and transmit more information while UAV-J moves closer to the eavesdroppers to get the best position for jamming accordingly.

In Fig. 2(b), for all given values of T, both UAV-S and UAV-J first fly to a lower altitude, then they cruise at the altitude for a certain period of time, and subsequently climbs up until reaching the final location. The reason is that the UAVs reduce the altitude to simultaneously come closer to the mobile user and the eavesdroppers, which leads to a smaller path loss between the UAV-S and the mobile user as well as a larger AN jamming between the UAV-J and the eavesdroppers, and thereby improves the system secrecy rate performance.

Fig. 3(a) and Fig. 3(b) plot the projections of the trajectories of the UAVs with the following four schemes, respectively: 1) The proposed robust 3D joint optimization (3D-joint.opt), i.e., $\Delta Q_1 = \Delta Q_2 = 20$ m; 2) The worst-robust 3D joint optimization (WRob-3D-joint.opt), i.e., $\Delta Q_1 = 100$ m and $\Delta Q_2 = 20$ m; 3) The robust 2D joint optimization (2D-joint.opt), i.e., $\Delta Q_1 = \Delta Q_2 = 20$ m and $h_u = 100$ m, $u \in \{s, j\}$; 4) The worst-robust 2D joint optimization (WRob-2D-joint.opt), i.e., $\Delta Q_1 = 100$ m and $h_u = 100$ m. From the simulation results illustrated in Fig. 3(a), when $\Delta Q_1 = \Delta Q_2 = 20$ m, the proposed 3D-joint.opt and 2D-joint.opt schemes yield similar aerial trajectories which is similar to Fig. 2(a). However, when the estimation error ΔQ_1 is sufficiently large, i.e., $\Delta Q_1 = 100$ m, the UAV-J in WRob-

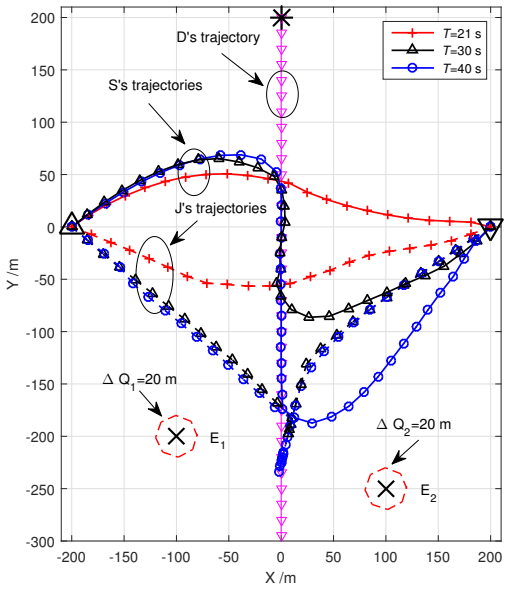

(a)

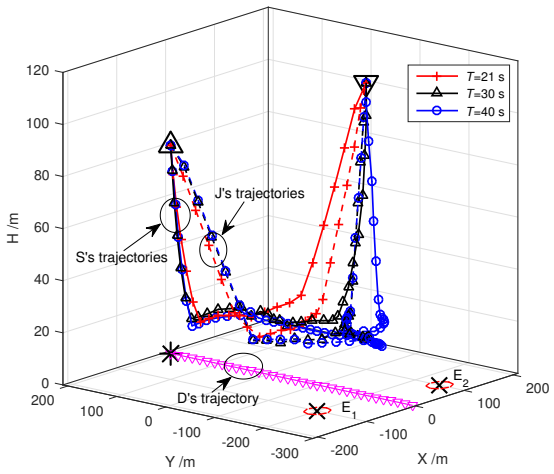

(b)

Fig. 2. Optimized UAVs trajectories during different time durations T: (a) Horizontal plane; (b) 3D plane

3D-joint.opt and WRob-2D-joint.opt schemes hover over the left of the center location of the eavesdroppers for a longer time duration compared to the above 3D-joint.opt and 2D-joint.opt schemes. The reason behind this behavior is that the eavesdropper E_1 can be closer to the mobile user with the increasing estimation error, and thus, the UAV-J is required to fly to the possible center location of the eavesdroppers to effectively transmit AN.

As in Fig. 2(b), similar 3D trajectories can be observed in Fig. 3(b). Nevertheless, different to the 2D schemes with the fixed flight altitude, both UAV-S and UAV-J in the proposed

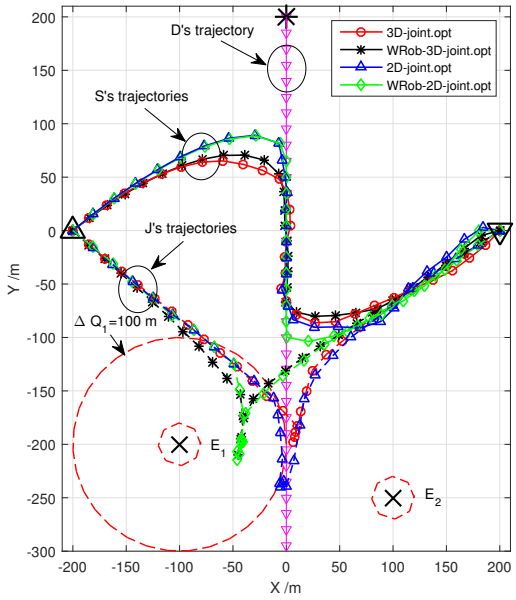

(a)

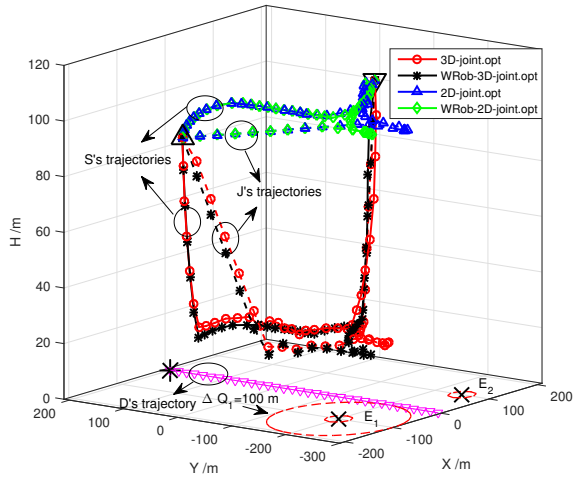

(b)

Fig. 3. Optimized UAVs trajectory of different algorithms with $T = 30$ s : (a) Horizontal plane; (b) 3D plane .

3D schemes can flexibly adjust their heights to obtain a better system performance, which is discussed in the following simulations.

Fig. 4 compares the performance of our proposed robust 3D joint design with that of the other four benchmark schemes with different flight time slots N, where a fixed TS ratio scheme (NTS-joint.opt) is considered, i.e., $\alpha[n] = 0.5$. As can be seen in Fig. 4, the average secrecy rate of all schemes first increases and then decreases slowly as the number of the flight time slots N increases. This is because when N is small, increasing the flight time slots would result in a higher SINR

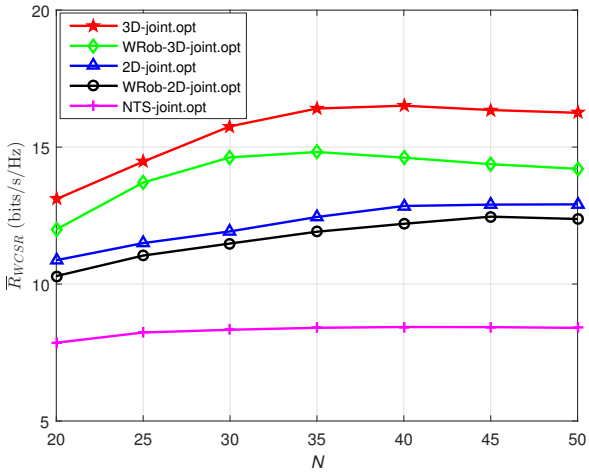

Fig. 4. Achieved average secrecy rates of different algorithms versus N.

at the mobile user and a lower SINR at the eavesdroppers due to the UAVs position closer to them. However, when N is large enough, the mobile user moves closer to the location of the eavesdroppers, which results in more information intercepted at the eavesdroppers. Furthermore, as expected, the proposed robust 3D algorithm achieves a superior performance compared to that of the 2D-joint.opt and NTS-joint.opt schemes. The reason for this superior performance is that the proposed 3D joint design can effectively exploit the available more degrees of freedom of the UAV's horizontal and vertical locations as well as the TS ratio. Furthermore, when the estimation error ΔQ_1 is large, it is obvious that the achievable average secrecy rate performance of the WRob-3D-joint.opt and WRob-2D-joint.opt schemes is worse than that of the 3D-joint.opt and 2D-joint.opt schemes, respectively. This is because the uncertainty of eavesdroppers' locations is larger for a larger ΔQ_k, and the trajectory design and resource allocation, in turn, would be more conservative; this leads to a less efficient utilization of the system resources.

Next, we show the achievable average secrecy rates of the aforementioned five schemes versus different transmit power $P_s[n] = P_j[n]$ with $N = 30$. From the simulation results illustrated in Fig. 5, as expected, the achievable average secrecy rate of all schemes increases as the transmit power at UAV-S and UAV-J increases. The reason behind this behavior is that increasing the transmit power $P_s[n] = P_j[n]$ can improve the instantaneous $\mathrm{SINR_d}$ at the user and simultaneously deteriorate the corresponding $\mathrm{SINR_e}$ quickly at the eavesdroppers. Furthermore, as can be seen in Fig. 5, the proposed robust 3D algorithm always shows significant performance gain over the other four benchmark schemes for any given value of $P_s[n] = P_j[n]$, which has been previously explained in detail.

In Fig. 6, we investigate the convergence of the proposed algorithm and the four benchmark algorithms with $N = 30$. As can be seen in Fig. 6, the achievable average secrecy rates of all algorithms first increase with the number of iterations in

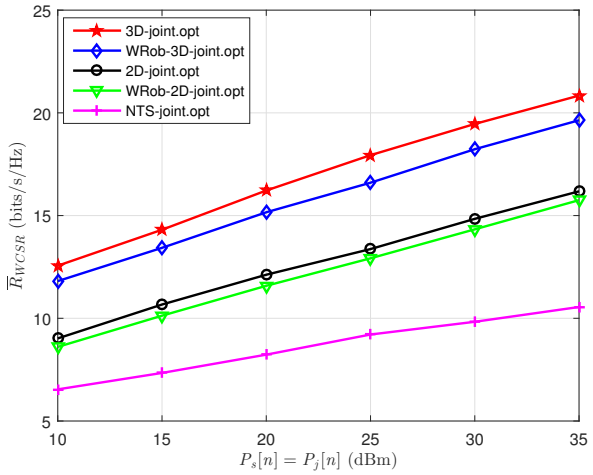

Fig. 5. Achieved average secrecy rates of different algorithms versus $P_s[n] = P_j[n]$.

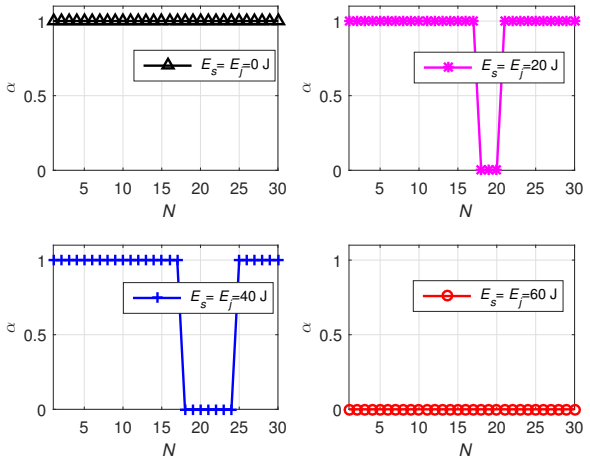

Fig. 7. TS resource profile of different EH thresholds versus N.

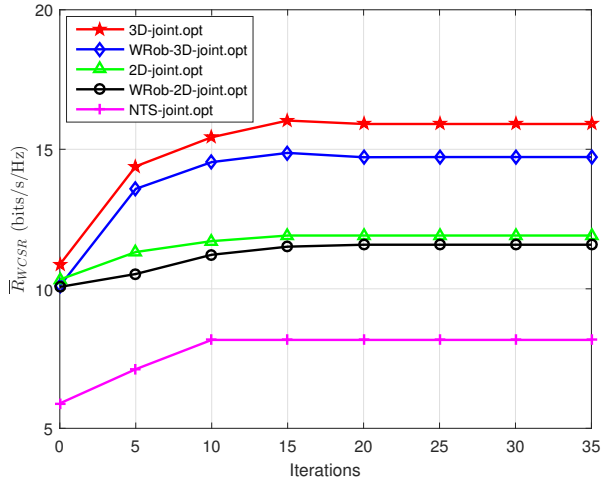

Fig. 6. Convergence of different algorithms.

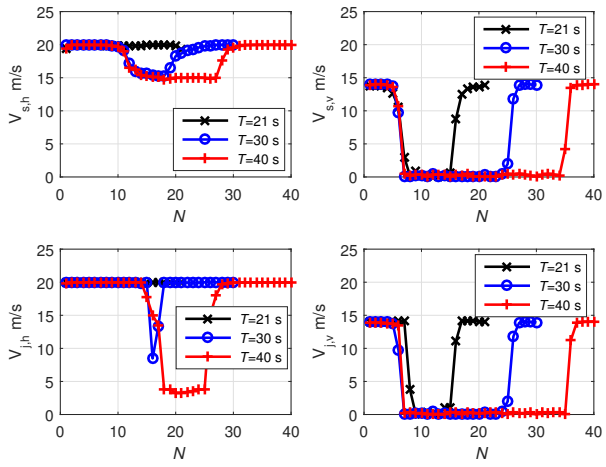

Fig. 8. Flight velocity of UAVs with different time durations against N.

Table II, and then converge to a constant secrecy rate within a few iterations. In addition, it is also observed that the speed of convergence of the proposed 3D scheme is similar to that of the other benchmark schemes. Furthermore, from Fig. 6, it is noticed that the proposed algorithm converges within 20 iterations on average.

Fig. 7 illustrates the TS resource profile of UAVs versus different flight time N and EH threshold E_u, $u \in \{s, j\}$. As shown in Fig. 7, when E_u is small, i.e., $E_s = E_j = 0$ J, the UAVs remain with the TS ratio $\alpha = 1$ for different N values. This implies that all time slots are used for information transmission. As E_u increases, i.e., $E_s = E_j = 20$ J and $E_s = E_j = 40$ J, both UAV-S and UAV-J reduce the TS ratio to zero for a certain period of time such that sufficient energy can be harvested. Thus, the UAVs need to design the optimal TS resource profile in an energy-constrained system to achieve the best system performance. In addition, as can be seen in Fig. 7, when the EH requirement at the UAVs is large enough, i.e., $E_s = E_j = 60$ J, the UAVs will keep the TS ratio $\alpha = 0$ unchanged as N increases. This is because both UAV-S and UAV-J need to harvest energy among all time slots to meet the EH requirements.

Finally, we present the UAVs' horizontal and vertical velocity, $V_{u,h}$ and $V_{u,v}$, $u \in \{s, j\}$, versus different time durations N, respectively. As shown in Fig. 8 (top left), when T is small, i.e., $T = 21$ s, the UAV-S flies to the final location with the maximum horizontal speed $V_{s,h}^{max} = 20$ m/s. However, when T is large (e.g., $T = 30$ and $T = 40$ s), the UAV-S first flies at its maximum horizontal speed to get closer to the mobile user. Then, it reduces the horizontal speed to 15 m/s to follow the user ($V_d^{max} = 15$ m/s) as long as possible, and finally flies to the final location with maximum horizontal speed. From Fig. 8 (top right), for all considered T values, the UAV-S quickly reduces the vertical speed to 0 and then cruises at the vertical speed before reaching the final location. This is because a large vertical speed may lead to a large vertical displacement

which causes a large path loss of the communication links and a degradation of the system performance. Furthermore, as can be seen in Fig. 8 (bottom left), the UAV-J first flies with the maximum horizontal speed and then reduces the horizontal speed to a lower value until reaches the final location as N increases. The reason behind this behavior is that the UAV-J needs to find its optimum position quickly and then hovers at that position near the eavesdroppers as long as possible for jamming purpose. In addition, from Fig. 8 (bottom right), the UAV-J follows a vertical speed policy during all time slots N similar to that of the UAV-S. This is because that the UAV-J can cruise at lowest altitude with vertical speed $V_{j,v} = 0$ $\mathrm{m/s}$, which results in a more effective AN jamming to the eavesdroppers.

V. Conclusion

In this paper, we have investigated the jointly optimal 3D-trajectory and TS allocation design for energy-constrained dual-UAV-assisted secure communication systems with imperfect eavesdropper locations. We have formulated an optimization problem to maximize the worst-case secrecy rate from the UAVs to the mobile user among all time slots under the UAV's mobility, anti-collision, positioning and EH constraints. Different from the most previous works which use the free space path loss model to simplify the analysis, we have adopted a typical UAV-ocean channel model with both large-scale and small-scale fading components. In order to deal with the non-convexity issue, we have first decomposed the original optimization problem into three subproblems and then transformed them into more tractable forms. Finally, we have developed an iterative algorithm to determine a suboptimal solution of the considered problem. Furthermore, we have analyzed the convergence and the impact of different parameters of the proposed algorithm. The simulation results have demonstrated that the proposed 3D dual-UAV joint design can achieve a significant improvement in average secrecy rate compared to conventional 2D UAV-aided schemes.

Appendix A
Transformation of constraint (23b)

Let us first substitute (4) and (5) into (23b) and rewrite it as

$$\Delta x_k^2[n] + \Delta y_k^2[n] - \Delta Q_k^2 \le 0, \forall k, \tag{35a}$$

$$-(x_s[n]-x_{e_k}[n]-\Delta x_k[n])^2-(y_s[n]-y_{e_k}[n]-\Delta y_k[n])^2 - h_s^2[n] + t_2[n] \le 0, \forall k. \tag{35b}$$

By exploiting the S-Procedure [23], [46], [47], the constraint (23b) can be rewritten as follows:

$$\mathbf{\Phi}(x_s[n], y_s[n], h_s[n], t_2[n], \xi_k[n]) \succeq 0, \forall k, n, \tag{36}$$

where $\mathbf{\Phi}(x_s[n], y_s[n], h_s[n], t_2[n], \xi_k[n]) = \begin{bmatrix} \xi_k[n]+1 & 0 & x_{e_k}[n]-x_s[n] \\ 0 & \xi_k[n]+1 & y_{e_k}[n]-y_s[n] \\ x_{e_k}[n]-x_s[n] & y_{e_k}[n]-y_s[n] & -\Delta Q_k^2\xi_k[n]+c_k[n] \end{bmatrix}$, and $c_k[n] = x_s^2[n] - 2x_{e_k}[n]x_s[n] + x_{e_k}^2[n] + y_s^2[n] - 2y_{e_k}[n]y_s[n] + y_{e_k}^2[n] + h_s^2[n] - t_2[n]$. Since the terms $x_s^2[n]$, $y_s^2[n]$ and $h_s^2[n]$ contained in $c_k[n]$ are non-linear, by using the first-order Taylor series expansions of them, we have

$$\begin{aligned} x_s^2[n] &\ge -x_{s_{fea}}^2[n] + 2x_{s_{fea}}[n]x_s[n], \\ y_s^2[n] &\ge -y_{s_{fea}}^2[n] + 2y_{s_{fea}}[n]y_s[n], \\ h_s^2[n] &\ge -h_{s_{fea}}^2[n] + 2h_{s_{fea}}[n]h_s[n], \end{aligned} \tag{37}$$

where $\mathbf{x}_{s_{fea}} \triangleq [x_{s_{fea}}[1], x_{s_{fea}}[2], ..., x_{s_{fea}}[N]]^\dagger$, $\mathbf{y}_{s_{fea}} \triangleq [y_{s_{fea}}[1], y_{s_{fea}}[2], ..., y_{s_{fea}}[N]]^\dagger$, and $\mathbf{h}_{s_{fea}} \triangleq [h_{s_{fea}}[1], h_{s_{fea}}[2], ..., h_{s_{fea}}[N]]^\dagger$. Thus, the constraint (36) can be equivalently converted as

$$\widetilde{\mathbf{\Phi}}(x_s[n], y_s[n], h_s[n], t_2[n], \xi_k[n]) \succeq 0, \forall k, n, \tag{38}$$

where $\widetilde{\mathbf{\Phi}}(x_s[n], y_s[n], h_s[n], t_2[n], \xi_k[n]) = \begin{bmatrix} \xi_k[n]+1 & 0 & x_{e_k}[n]-x_s[n] \\ 0 & \xi_k[n]+1 & y_{e_k}[n]-y_s[n] \\ x_{e_k}[n]-x_s[n] & y_{e_k}[n]-y_s[n] & -\Delta Q_k^2\xi_k[n]+\widetilde{c}_k[n] \end{bmatrix}$, and $\widetilde{c}_k[n] = -x_{s_{fea}}^2[n] + 2x_{s_{fea}}[n]x_s[n] - 2x_{e_k}[n]x_s[n] + x_{e_k}^2[n] - y_{s_{fea}}^2[n] + 2y_{s_{fea}}[n]y_s[n] - 2y_{e_k}[n]y_s[n] + y_{e_k}[n]^2 - h_{s_{fea}}^2[n] + 2h_{s_{fea}}[n]h_s[n] - t_2[n]$. This completes the proof.

Appendix B
The convergence analysis of the proposed algorithm in Table II

Suppose $\Psi\{\boldsymbol{\alpha}^{l-1}, \boldsymbol{u}_s^{l-1}, \boldsymbol{u}_j^{l-1}\}$ denotes the objective value of the problem in (13) in the $(l-1)$-th iteration, where $\boldsymbol{u}_s^{l-1} = (x_s^{l-1}, y_s^{l-1}, h_s^{l-1})$ and $\boldsymbol{u}_j^{l-1} = (x_j^{l-1}, y_j^{l-1}, h_j^{l-1})$. First, in step 5 of Table II, since the optimal solution of problem in (20) is obtained for given $\boldsymbol{u}_s^{l-1}$ and $\boldsymbol{u}_j^{l-1}$, we have

$$\Psi\{\boldsymbol{\alpha}^{l-1}, \boldsymbol{u}_s^{l-1}, \boldsymbol{u}_j^{l-1}\} \le \Psi\{\boldsymbol{\alpha}^{l}, \boldsymbol{u}_s^{l-1}, \boldsymbol{u}_j^{l-1}\}, \tag{39}$$

where $\Psi\{\boldsymbol{\alpha}^{l}, \boldsymbol{u}_s^{l-1}, \boldsymbol{u}_j^{l-1}\}$ denotes the computed objective value of problem in (20). Second, for given $\boldsymbol{\alpha}^l$ and $\boldsymbol{u}_j^{l-1}$ in step 6 of Table II, it follows that

$$\begin{aligned} \Psi\{\boldsymbol{\alpha}^{l}, \boldsymbol{u}_s^{l-1}, \boldsymbol{u}_j^{l-1}\} &\overset{(a)}{=} \Psi_s^{lb}\{\boldsymbol{\alpha}^{l}, \boldsymbol{u}_s^{l-1}, \boldsymbol{u}_j^{l-1}\} \\ &\overset{(b)}{\le} \Psi_s^{lb}\{\boldsymbol{\alpha}^{l}, \boldsymbol{u}_s^{l}, \boldsymbol{u}_j^{l-1}\} \\ &\overset{(c)}{\le} \Psi\{\boldsymbol{\alpha}^{l}, \boldsymbol{u}_s^{l}, \boldsymbol{u}_j^{l-1}\}, \end{aligned} \tag{40}$$

where Ψ_s^{lb} represents the objective value of problem in (27), (a) is due to the tightness of the first-order Taylor series expansions at local points in the problem in (27), (b) holds since the problem in (27) is solved optimally for given $\boldsymbol{\alpha}^l$ and $\boldsymbol{u}_j^{l-1}$, and (c) holds due to the fact that the optimal objective value of problem in (27) is the lower bound of that of the problem in (22). Similarly, for given $\boldsymbol{\alpha}^l$ and $\boldsymbol{u}_s^l$ in step 7 of Table II, we have

$$\begin{aligned} \Psi\{\boldsymbol{\alpha}^{l}, \boldsymbol{u}_s^{l}, \boldsymbol{u}_j^{l-1}\} &\overset{(d)}{=} \Psi_j^{lb}\{\boldsymbol{\alpha}^{l}, \boldsymbol{u}_s^{l}, \boldsymbol{u}_j^{l-1}\} \\ &\overset{(e)}{\le} \Psi_j^{lb}\{\boldsymbol{\alpha}^{l}, \boldsymbol{u}_s^{l}, \boldsymbol{u}_j^{l}\} \\ &\overset{(f)}{\le} \Psi\{\boldsymbol{\alpha}^{l}, \boldsymbol{u}_s^{l}, \boldsymbol{u}_j^{l}\}. \end{aligned} \tag{41}$$

Thus, combing (39)−(41), we can obtain that

$$\Psi\{\boldsymbol{\alpha}^{l-1}, \boldsymbol{u}_s^{l-1}, \boldsymbol{u}_j^{l-1}\} \leq \Psi\{\boldsymbol{\alpha}^{l}, \boldsymbol{u}_s^{l}, \boldsymbol{u}_j^{l}\}, \tag{42}$$

which guarantees that the objective value of the problem in (13) is non-decreasing over the iterations. Thus, the solution obtained by the iterative algorithm in Table II can be guaranteed to converge to a suboptimal solution. This completes the proof.

REFERENCES

[1] Y. Zeng, R. Zhang, and J. L. Teng, "Wireless communications with unmanned aerial vehicles: Opportunities and challenges," *IEEE Commun. Mag.*, vol. 54, no. 5, pp. 36-42, Oct. 2016.

[2] W. Feng, J. Wang, Y. Chen, X. Wang, N. Ge, and J. Lu, "UAV-aided MIMO communications for 5G Internet of Things," *IEEE Internet Things J.*, vol. 6, no. 2, pp. 1731-1740, Apr. 2019.

[3] A. Masaracchia, L. D. Nguyen, T. Q. Duong, C. Yin, O. A. Dobre, and E. Garcia-Palacios, "Energy-efficient and throughput fair resource allocation for TS-NOMA UAV-assisted communications," *IEEE Trans. Commun.*, vol. 68, no. 11, pp. 7156-7169, Nov. 2020.

[4] A. Al-Habob, O. A. Dobre, S. Muhaidat, and H. V. Poor, "Energy-efficient data dissemination using a UAV: An ant colony approach," *IEEE Wireless Commun. Lett.*, vol. 10, no. 1, pp. 16-20, Jan. 2021.

[5] Q. Wu, L. Liu, and R. Zhang, "Fundamental trade-offs in communication and trajectory design for UAV-enabled wireless network," *IEEE Wireless Commun.*, vol. 26, no. 1, pp. 36-44, Feb. 2019.

[6] Y. Zeng and R. Zhang, "Energy-efficient UAV communication with trajectory optimization," *IEEE Trans. Wireless Commun.*, vol. 16, no. 6, pp. 3747-3760, Jun. 2017.

[7] Y. Chen, W. Feng, and G. Zheng, "Optimum placement of UAV as relays," *IEEE Commun. Lett.*, vol. 22, no. 2, pp. 248-251, Feb. 2018.

[8] Z. Kaleem, S. Shakoor, D. T. Do, O. A. Dobre, and A. Jamalipour, "Joint optimization of UAV 3D placement and path loss factor for energy efficient maximal coverage," *IEEE Internet Things J.*, to be published.

[9] X. Sun, D. W. K. Ng, Z. Ding, Y. Xu, and Z. Zhong, "Physical layer security in UAV systems: Challenges and opportunities," *IEEE Wireless Commun.*, vol. 26, no. 5, pp. 40-47, Oct. 2019.

[10] X. Chen, D. W. K. Ng, W. H. Gerstackera, and H. Chen, "A survey on multiple-antenna techniques for physical layer security," *IEEE Commun. Surveys Tuts.*, vol. 19, no. 2, pp. 1027-1053, Nov. 2017.

[11] K. Cumanan, G. C. Alexandropoulos, Z. Ding, and G. K. Karagiannidis, "Secure communications with cooperative jamming: Optimal power allocation and secrecy outage analysis," *IEEE Trans. Veh. Technol.*, vol. 66, no. 8, pp. 7495-7505, Aug. 2017.

[12] K. Cumanan, Z. Ding, M. Xu, and H. V. Poor, "Secrecy rate optimization for secure multicast communications," *IEEE J. Sel. Topics Signal Process.*, vol. 10, no. 8, pp. 1417-1432, Dec. 2016.

[13] P. Xu, K. Cumanan, Z. Ding, X. Dai, and K. K. Leung, "Group secret key generation in wireless networks: Algorithms and rate optimization," *IEEE Trans. Inf. Forensics and Security*, vol. 11, no. 8, pp. 1831-1846, Aug. 2016.

[14] X. Li, W. Wang, M. Zhang, F. Zhou, and N. AI-Dhahir, "Robust secure beamforming for SWIPT-aided relay systems with full-duplex receiver and imperfect CSI," *IEEE Trans. Veh. Technol.*, vol. 69, no. 2, pp. 1867-1878, Feb. 2020.

[15] H. Wang, X. Zhang, and J. Jiang, "UAV-involved wireless physical-layer secure communications: Overview and research directions," *IEEE Wireless Commun.*, vol. 26, no. 5, pp. 32-39, Oct. 2019.

[16] Q. Wu, W. Mei, and R. Zhang, "Safeguarding wireless network with UAVs: A physical layer security perspective," *IEEE Wireless Commun.*, vol. 26, no. 5, pp. 12-18, Oct. 2019.

[17] Q. Wang, Z. Chen, W. Mei, and J. Fang, "Improving physical layer security using UAV-enabled mobile relaying," *IEEE Wireless Commun. Lett.*, vol. 6, no. 3, pp. 310-313, Jun. 2017.

[18] G. Zhang, Q. Wu, M. Cui, and R. Zhang, "Securing UAV communications via trajectory optimization," in *Proc. IEEE Global Communications Conference (GLOBECOM)*, pp. 1-6, Singapore, Singapore, Dec. 2017.

[19] G. Zhang, Q. Wu, M. Cui, and R. Zhang, "Securing UAV communications via joint trajectory and power control," *IEEE Trans. Wireless Commun.*, vol. 18, no. 2, pp. 1376-1389, Feb. 2019.

[20] A. Li, Q. Wu, and R. Zhang, "UAV-enabled cooperative jamming for improving secrecy of ground wiretap channel," *IEEE Wireless Commun. Lett.*, vol. 8, no. 1, pp. 181-184, Jan. 2019.

[21] K. Xu, M. Zhao, Y. Cai, and L. Hanzo, "Low-complexity joint power allocation and trajectory design for UAV-enabled secure communications with power splitting," *IEEE Trans. Commun.*, vol. 69, no. 3, pp. 1896-1911, Mar. 2021.

[22] X. Hong, P. Liu, F. Zhou, S. Guo, and Z. Chu, "Resource allocation for secure UAV-assisted SWIPT systems," *IEEE Access,* vol. 7, pp. 24248-24257, Feb. 2019.

[23] M. Cui, G. Zhang, Q. Wu and D. W. K. Ng, "Robust trajectory and transmit power design for secure UAV communications," *IEEE Trans. Veh. Technol.*, vol. 67, no. 9, pp. 9042-9046, Sep. 2018.

[24] Y. Cai, F. Cui, Q. Shi, M. Zhao, and G. Y. Li, "Dual-UAV-enabled secure communications: Joint trajectory design and user scheduling," *IEEE J. Sel. Areas Commun.*, vol. 36, no. 9, pp. 1972-1985, Sep. 2018.

[25] H. Lee, S. Eom, J. Park, and I. Lee, "UAV-aided secure communications with cooperative jamming," *IEEE Trans. Veh. Technol.*, vol. 67, no. 10, pp. 9385-9392, Oct. 2018.

[26] X. Zhou, Q. Wu, S. Yan, F. Shu, and J. Li, "UAV-enabled secure communications: Joint trajectory and transmit power optimization," *IEEE Trans. Veh. Technol.*, vol. 68, no. 4, pp. 4069-4073, Apr. 2019.

[27] C. You and R. Zhang, "3D trajectory optimization in rician fading for UAV-enabled data harvesting," *IEEE Trans. Wireless Commun.*, vol. 18, no. 6, pp. 3192-3207, Jun. 2019.

[28] Y. Sun, D. Xu, D. W. K. Ng, L. Dai, and R. Schober, "Optimal 3D-trajectory design and resource allocation for solar-powered UAV communication systems," *IEEE Trans. Commun.*, vol. 67, no. 6, pp. 4281-4298, Jun. 2019.

[29] Y. Guo, S. Yin, and J. Hao, "Resource allocation and 3D trajectory design in wireless networks assisted by rechargeable UAV," *IEEE Wireless Commun. Lett.*, vol. 8, no. 3, pp. 781-784, Jun. 2019.

[30] W. Feng, N. Zhao, S. Ao, J. Tang, X. Zhang, Y. Fu, D. K. C. So, and K. K. Wong, "Joint 3D trajectory design and time allocation for UAV-enabled wireless power transfer networks, " *IEEE Trans. Veh. Technol.*, vol. 69, no. 9, pp. 9265-9278, Sep. 2020.

[31] Y. Huang, W. Mei, J. Xu, L. Qiu, and R. Zhang, "Cognitive UAV communication via joint maneuver and power control," *IEEE Trans. Commun.*, vol. 67, no. 11, pp. 7872-7888, Nov. 2019.

[32] J. Yao, C. Zhong, Z. Liu, and J. Xu, "3D trajectory optimization for secure UAV communication with CoMP reception," in *Proc. IEEE Global Communications Conference (GLOBECOM)*, pp. 1-6, Hawaii, USA, Dec. 2019.

[33] X. Li, W. Feng, Y. Chen, C. Wang and N. Ge, "Maritime coverage enhancement using UAVs coordinated with hybrid satellite-terrestrial networks," *IEEE Trans. Commun.*, vol. 68, no. 4, pp. 2355-2369, Apr. 2020.

[34] X. Li, W. Feng, J. Wang, Y. Chen, N. Ge, and C. Wang, "Enabling 5G on the ocean: A hybrid satellite-UAV-terrestrial network solution," *IEEE Wireless Commun.*, vol. 27, no. 6, pp. 116-121, Dec. 2020.

[35] M. Zhao, Q. Shi, and M. Zhao, "Efficiency maximization for UAV-enabled mobile relaying systems with laser charging," *IEEE Trans. Wireless Commun.*, vol. 19, no. 5, pp. 3257-3272, May 2020.

[36] S. Yin, J. Tan, and L. Li, "UAV-assisted cooperative communications with time-sharing SWIPT," in *Proc. IEEE International Conference on Communications (ICC)*, pp. 20-24, Kansas City, USA, May 2018.

[37] B. Ji, Y. Li, B. Zhou, C. Li, K. Song, and H. Wen, "Performance analysis of UAV relay assisted IoT communication network enhanced with energy harvesting," *IEEE Access,* vol. 7, pp. 38738-38747, Mar. 2019.

[38] W. Wang, X. Li, M. Zhang, K. Cumanan, D. W. K. Ng, G. Zhang, J. Tang, and O. A. Dobre, "Energy-constrained UAV-assisted secure communications with position optimization and cooperative jamming," *IEEE Trans. Commun.*, vol. 68, no. 7, pp. 4476-4489, Jul. 2020.

[39] A. Danjo and S. Hara, "Optimal formation of unmanned aerial vehicles for minimizing localization error-A two-dimensional case," in *Proc. IEEE Workshop on Signal Processing Advances in Wireless Communications (SPAWC)*, pp. 1-4, Sapporo, 2017.

[40] M. Farkas, B. Vanek, and S. Rozsa, "Small UAV's position and attitude estimation using tightly coupled multi baseline multi constellation

GNSS and inertial sensor fusion," in *Proc. IEEE Workshop on Metrology for AeroSpace (MetroAeroSpace)*, pp. 176-181, Torino, Italy, 2019.
[41] C. R. Valenta and G. D. Durgin, "Harvesting wireless power: survey of energy-harvester conversion efficiency in far-field, wireless power transfer systems," *IEEE Microw. Mag.*, vol. 15, no. 4, pp. 108-120, Jun. 2014.
[42] E. Boshkovska, D. W. K. Ng, N. Zlatanov, and R. Schober, "Practical non-linear energy harvesting model and resource allocation for SWIPT systems," *IEEE Commun. Lett.*, vol. 19, no. 12, pp. 2082-2085, Dec. 2015.
[43] Y. Zeng, B. Clerckx, and R. Zhang, "Communications and signals design for wireless power transmission," *IEEE Trans. Commun.*, vol. 65, no. 5, pp. 2264-2290, May 2017.
[44] C. Zhan, Y. Zeng, and R. Zhang, "Energy-efficient data collection in UAV enabled wireless sensor network," *IEEE Wireless Commmu. Lett.*, vol. 7, no. 3, pp. 328-331, Jun. 2018.
[45] Q. Wu, Y. Zeng, and R. Zhang, "Joint trajectory and communication design for multi-UAV enabled wireless networks," *IEEE Trans. Wireless Commun.*, vol. 17, no. 3, pp. 2109-2121, Mar. 2018.
[46] S. Boyd and L. Vandenberghe, *Convex Optimization*. Cambridge, U.K.: Cambridge Univ. Press, 2004.
[47] Y. Li, R. Zhang, J. Zhang, S. Gao, and L. Yang, "Cooperative jamming for secure UAV communications with partial eavesdropper information," *IEEE Access*, vol. 7, pp. 94593-94603, Jul. 2019.
[48] M. Grant and S. Boyd, *CVX: Matlab Software for Disciplined Convex Programming*, Jul. 2010 [Online]. Available: http://cvxr.com/cvx.
[49] A. Ben-Tal and A. Nemirovski, *Lectures on Modern Convex Optimization: Analysis, Algorithms, and Engineering Applications (MPS-SIAM Series on Optimization)*. Philadelphia, PA, USA: SIAM, 2001.

Wei Wang (Member, IEEE) received the Ph.D. degree in communication and information system from Shanghai University, Shanghai, China, in 2011. He is currently an Associate Professor with the School of Information Science and Technology, Nantong University. He is also with the Peng Cheng Laboratory and the Nantong Research Institute for Advanced Communication Technologies. From Feb. 2016 to Aug. 2016, he was a Visiting Scholar in the Department of Electrical and Computer Engineering at the Boise State University, ID, USA. From Feb. 2019 to Aug. 2019, he was an Academic Visitor in the Department of Electronic Engineering at the University of York, York, UK. His current research interests include unmanned aerial vehicle communications, maritime communications, physical layer security, and machine learning for wireless communications.

Xinrui Li received the B.S. degree in electronic and information engineering from Nantong University, China, in 2018, where he is currently pursuing the M.S. degree in information and communication engineering. His research interests include unmanned aerial vehicle communications, physical layer security, and wireless information and power transfer.

Rui Wang (Senior Member, IEEE) received the Ph.D. degree from Shanghai Jiao Tong University, China, in 2013. From August 2012 to February 2013, he was a Visiting Ph.D. Student with the Department of Electrical Engineering, University of California at Riverside. From October 2013 to October of 2014, he was with the Institute of Network Coding, The Chinese University of Hong Kong, as a Post-Doctoral Research Associate. From October 2014 to December 2016, he was with the College of Electronics and Information Engineering, Tongji University, as an Assistant Professor, where he is currently an Associate Professor.

Dr. Wang received the Shanghai Excellent Doctor Degree Dissertation Award in 2015 and received the ACM Shanghai Rising Star Nomination Award in 2016. He has published over 60 articles. His research interests include wireless communications, artificial intelligence and wireless positioning. He is currently an Associate Editor of IEEE ACCESS and an Editor of the IEEE WIRELESS COMMUNICATIONS LETTERS.

Kanapathippillai Cumanan (Senior Member, IEEE) received the BSc degree with first class honors in electrical and electronic engineering from the University of Peradeniya, Sri Lanka in 2006 and the PhD degree in signal processing for wireless communications from Loughborough University, Loughborough, UK, in 2009.

He is currently a Senior Lecturer with the Department of Electronic Engineering, University of York, York, UK. From March 2012 to November 2014, he was working as a research associate at School of Electrical and Electronic Engineering, Newcastle University, UK. Prior to this, he was with the School of Electronic, Electrical and System Engineering, Loughborough University, UK. In 2011, he was an academic visitor at Department of Electrical and Computer Engineering, National University of Singapore, Singapore. From January 2006 to August 2006, he was an assistant lecturer with Department of Electrical and Electronic Engineering, University of Peradeniya, Sri Lanka. His research interests include non-orthogonal multiple access (NOMA), cell-free massive MIMO, physical layer security, cognitive radio networks, convex optimization techniques and resource allocation techniques. He has published more than 100 journal articles and conference papers which attracted more than 2300 Google scholar citations. He is currently an Associate Editor of the IEEE OPEN JOURNAL OF THE COMMUNICATIONS SOCIETY and IEEE ACCESS, and an Editor of the IEEE WIRELESS COMMUNICATIONS LETTERS.

Wei Feng (Senior Member, IEEE) received the B.S. and Ph.D. degrees from the Department of Electronic Engineering, Tsinghua University, Beijing, China, in 2005 and 2010, respectively. He is currently an Associate Professor with the Department of Electronic Engineering, Tsinghua University. His research interests include maritime communication networks, large-scale distributed antenna systems, and coordinated satellite-UAV-terrestrial networks. He serves as the Assistant to the Editor-in-Chief of CHINA COMMUNICATIONS and an Editor of IEEE TRANSACTIONS ON COGNITIVE COMMUNICATIONS AND NETWORKING.

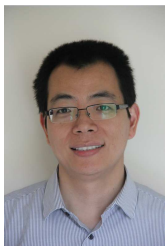

Zhiguo Ding (Fellow, IEEE) received his B.Eng in Electrical Engineering from the Beijing University of Posts and Telecommunications in 2000, and the Ph.D degree in Electrical Engineering from Imperial College London in 2005. From Jul. 2005 to Apr. 2018, he was working in Queen's University Belfast, Imperial College, Newcastle University and Lancaster University. Since Apr. 2018, he has been with the University of Manchester as a Professor in Communications. From Oct. 2012 to Sept. 2021, he has also been an Academic Visitor in Princeton University.

Dr Ding' research interests are 5G networks, game theory, cooperative and energy harvesting networks and statistical signal processing. He is serving as an Area Editor for the IEEE OPEN JOURNAL OF THE COMMUNICATIONS SOCIETY, an Editor for IEEE TRANSACTIONS ON VEHICULAR TECHNOLOGY, and JOURNAL OF WIRELESS COMMUNICATIONS AND MOBILE COMPUTING, and was an Editor for IEEE WIRELESS COMMUNICATION LETTERS, IEEE TRANSACTIONS ON COMMUNICATIONS, IEEE COMMUNICATION LETTERS from 2013 to 2016. He recently received the EU Marie Curie Fellowship 2012-2014, the Top IEEE TVT Editor 2017, IEEE Heinrich Hertz Award 2018, IEEE Jack Neubauer Memorial Award 2018, IEEE Best Signal Processing Letter Award 2018 , and Friedrich Wilhelm Bessel Research Award 2020. He is a Fellow of the IEEE, a Distinguished Lecturer of IEEE ComSoc, and a Web of Science Highly Cited Researcher in two categories 2020.

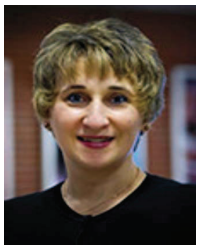

Octavia A. Dobre (Fellow, IEEE) received the Dipl. Ing. and Ph.D. degrees from the Polytechnic Institute of Bucharest, Romania, in 1991 and 2000, respectively. Between 2002 and 2005, she was with New Jersey Institute of Technology, USA. In 2005, she joined Memorial University, Canada, where she is currently a Professor and Research Chair. She was a Visiting Professor with Massachusetts Institute of Technology, USA and Université de Bretagne Occidentale, France. Her research interests encompass various wireless technologies, such as non-orthogonal multiple access and full duplex, as well as optical and underwater communications, and machine learning for communications. She has (co-)authored over 350 refereed papers in these areas.

Dr. Dobre serves as the Editor-in-Chief (EiC) of the IEEE OPEN JOURNAL OF THE COMMUNICATIONS SOCIETY. She was the EiC of the IEEE COMMUNICATIONS LETTERS, Senior Editor, Editor, and Guest Editor for various prestigious journals and magazines. She also served as General Chair, Technical Program Co-Chair, Tutorial Co-Chair, and Technical Co-Chair of symposia at numerous conferences.

Dr. Dobre was a Fulbright Scholar, Royal Society Scholar, and Distinguished Lecturer of the IEEE Communications Society. She obtained Best Paper Awards at various conferences, including IEEE ICC, IEEE Globecom, IEEE WCNC, and IEEE PIMRC. Dr. Dobre is a Fellow of the Engineering Institute of Canada.